COMPUTATIONAL MODELING OF DRUG RELEASE FROM NERVE GUIDE CONDUITS OF DIFFERENT DESIGNS

by

LOKESH SHAMKANT PATIL

Presented to the Faculty of the Graduate School of
The University of Texas at Arlington in Partial Fulfillment
of the Requirements
for the Degree of

MASTER OF SCIENCE IN BIOMEDICAL ENGINEERING

THE UNIVERSITY OF TEXAS AT ARLINGTON

May 2014

Acknowledgements

I would like to express my deepest gratitude to my committee members Dr. Eberhart, Dr. Chuong and Dr. Romero. I would like to thank Dr. Chuong for collaborating with Dr. Romero and helping me find a research topic and guiding me throughout the project work. I have learned a lot about interdisciplinary research through this project. I am thankful to my labmates Ishan and Jamie for their help with my thesis. I am especially thankful to Jamie for his help and insight with some of the concepts regarding finite element modeling. I would like to thank Nesreen who has worked on the experimental aspect of this project and shared her knowledge.

I am also grateful for the Bioengineering department faculty for giving me an opportunity to be part of their program. Finally and most importantly, I would like to thank my parents and brother, who have constantly supported me. Their patience and love is invaluable.

May 02, 2014

Abstract

COMPUTATIONAL MODELING OF DRUG RELEASE

FROM NERVE GUIDE CONDUITS

OF DIFFERENT DESIGNS

Lokesh Shamkant Patil, MS

The University of Texas at Arlington, 2014

Supervising Professor: Cheng-Jen Chuong

Currently there are limited effective strategies and surgical methods for repairing gap peripheral nerve injuries. Autografts are commonly used but with major limitation in the availability of donor graft material and the painful sensations at donor site. These limitations call for the development of new, effective methods for repairing peripheral nerve injuries. The use of nerve guide conduits to facilitate nerve growth and repair have shown promising potential with minimum side-effects but still with limited success in a full functional recovery. The likely clinical outcome could benefit significantly with the use of engineering methodologies in the design, fabrication, surgical delivery of the devices that maximize resulting effective nerve growth. In this study, we modeled the release of NGF growth factors in different designs of drug release conduits using finite element computational methods. Results show that the spatiotemporal concentration in models is significantly affected by design alterations. We also observe increase in axon linearity by changing coiling configuration and decreasing the NGC microchannel size. These models provide quantitative insights with time-varying NGF distribution in the microenvironment of the nerve guide conduits

Table of Contents

List of Illustrations

List of Tables

Nomenclature

1. NGC=Nerve guide conduit
2. PLGA=Poly lactic-co-glycolic acid
3. GF=Growth factor
4. RD=Radial Dispersion

Chapter 1

Introduction

1.1 Statistics and treatment

Around 360,000 people in United States suffer from upper extremity paralytic syndromes yearly[1]. This results in over 8.5 million restricted activity days and almost 5 million bed/disability days each year[1,2]. Moreover, peripheral nerve injuries can result in long-term partial or full impairment of limb function. To present day, peripheral nerve injuries present a strong challenge to surgeons and there is no “specific” method/technique or protocol for the needed repair. Various methods have been used depending on the nature and extent of the injury. Direct sutures for injury gaps < 5 mm can be performed. For gaps > 5 mm, often autologous grafts or less commonly, synthetic conduits are used. The functional recovery in case of conduits is most often sub-optimal[3]. Bridging injury gap with donor graft is often associated with many disadvantages. The method requires extra incisions for the removal of healthy sensory nerve[4]. Often autologous transplants are also associated with neuroma formation at the donor site[4]. Furthermore, long length nerve defects limit the availability of donor graft material[5]. As a result, extensive research has been undertaken in the last decade to understand nerve regeneration and the development of nerve conduit engineering.

1.2 How Nerve Conduits Work

Following a transection or gap injury, the functional recovery without any surgical aid is negligible because of death of cell bodies arising from retrograde effects, axon’s inability to find distal stump and ingrowing connective tissue[6].

In surgical procedures employing a nerve guidance conduit (NGC), the severed ends are introduced inside its lumen, and then fixed in place using sutures[6]. This use of conduit channel enclosure provides multiple benefits for nerve growth: it prevents any growth of surrounding tissues into the region and it allows for directional guidance for the neurites sprouting from proximal end. Furthermore, the enclosure preserves any trophic or growth factors that are released from the distal end. The outcome of using NGC can be evaluated by certain parameters. Among them, the most important ones are[6]:

- cross-sectional area of the regenerated nerve cable
- number of myelinated and unmyelinated axons
- percentages of cellular materials like epineurium, blood vessels, etc.
- electrophysiological and functional evaluation.

Figure 1-1 shows the procedure of surgical placement of tube for nerve repair[6]. While the use of an enclosed lumen is the general idea of NGC, a number of design variations can be been adopted to increase the efficiency of device performance. Usually neurotrophic factors are incorporated into the designs which support the survival, differentiation and growth of neurons[2]. The mechanism which governs the release of these growth factors can be different too. Growth factor can be simply embedded in the scaffold inside the channel lumen, or can be packaged into PLGA microsphere or drug eluting fibers. Currently, most NGCs are limited to adequately promote nerve regeneration if gap>1 cm for large diameter nerve and gap> 3cm for small diameter nerve[7]. Thus, there is a clear need for innovation in the design of NGCs for optimizing and maximizing the axon promoting potential. The use of engineering methodology offers this new promise.

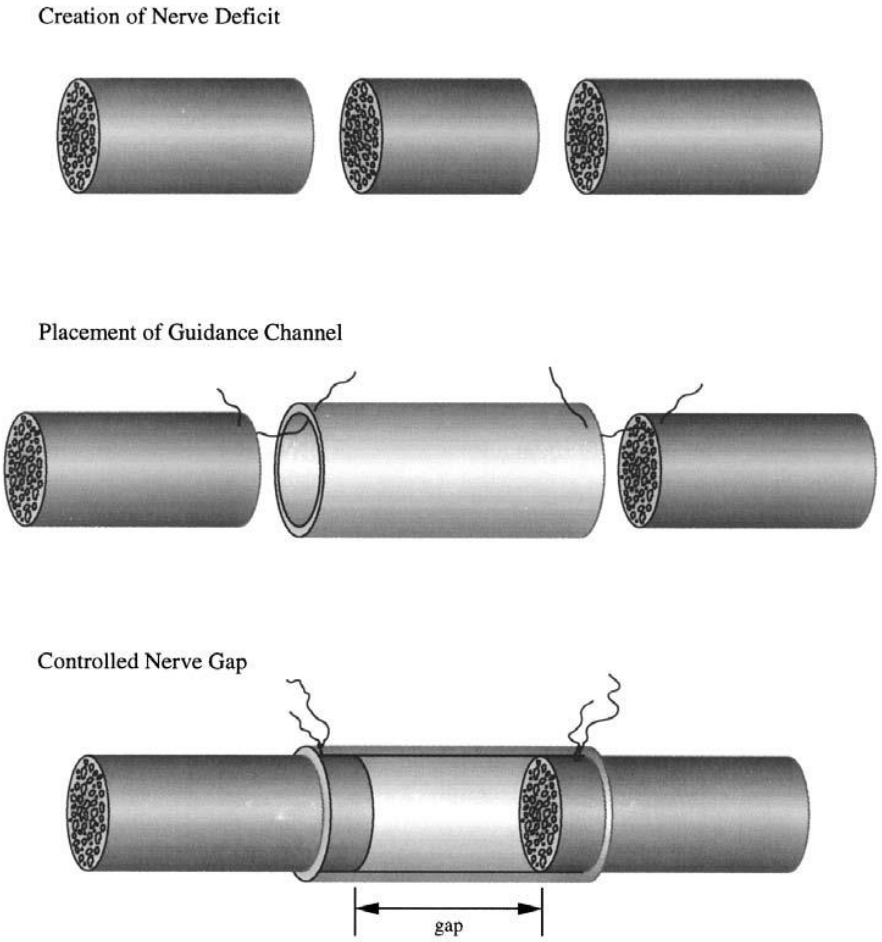

Figure 1-1 Illustration of tube repair procedure for treating peripheral injuries. An enclosed tube is used to connect the gap between the nerve ends.

1.3 Different designs modeled in this study

In this study, we compared the efficacy of drug release from six different designs used to promote the growth of severed nerve ends using channel lumen design (Figure 1-2). We then focus on the coiled drug delivery design (Case 3, 6) and examine the effect of parameters such as pitch and size of microchannel on the performance of device. For

defining the “performance” of device, we developed a protocol for quantifying the straightness of axon.

All designs used in the study use collagen scaffolding inside the main channel lumen. Collagen is usually preferred because of its microstructure which allows molecular diffusion and controlled resorption[8]. For Case 1 and 4, there is no release mechanism since the growth factors are uniformly embedded in the collagen scaffold. Case 2 and 4 used PLGA microspheres (diameter of 5 um) which allowed for controlled release of GFs. Case 3 and 6 also allow controlled release from ELUTE™ coil fiber. Because of differential coiling in Case 3 and 6, an axial chemotactic gradient is created. Former studies have demonstrated that axons can be guided directionally by a chemotactic gradient[9]. Case 4, 5, and 6 are variants of the first three cases with the introduction of multichannel design. It has been shown previously that multichannel conduits are more effective than single channel conduits and can possibly be used as an alternative to autografts[10].

Since modeling hundreds of microspheres would be computationally expensive, it was approximated that only 63 PLGA microspheres in Case 2 and 35 in Case 5 are present. The particles were placed in group of 9 in 7 different x-y planes for Case 2 throughout the length of channel. The particles were grouped in group of 5 in 7 x-y planes for Case 5. The placement pattern is depicted in Figure 1-3.

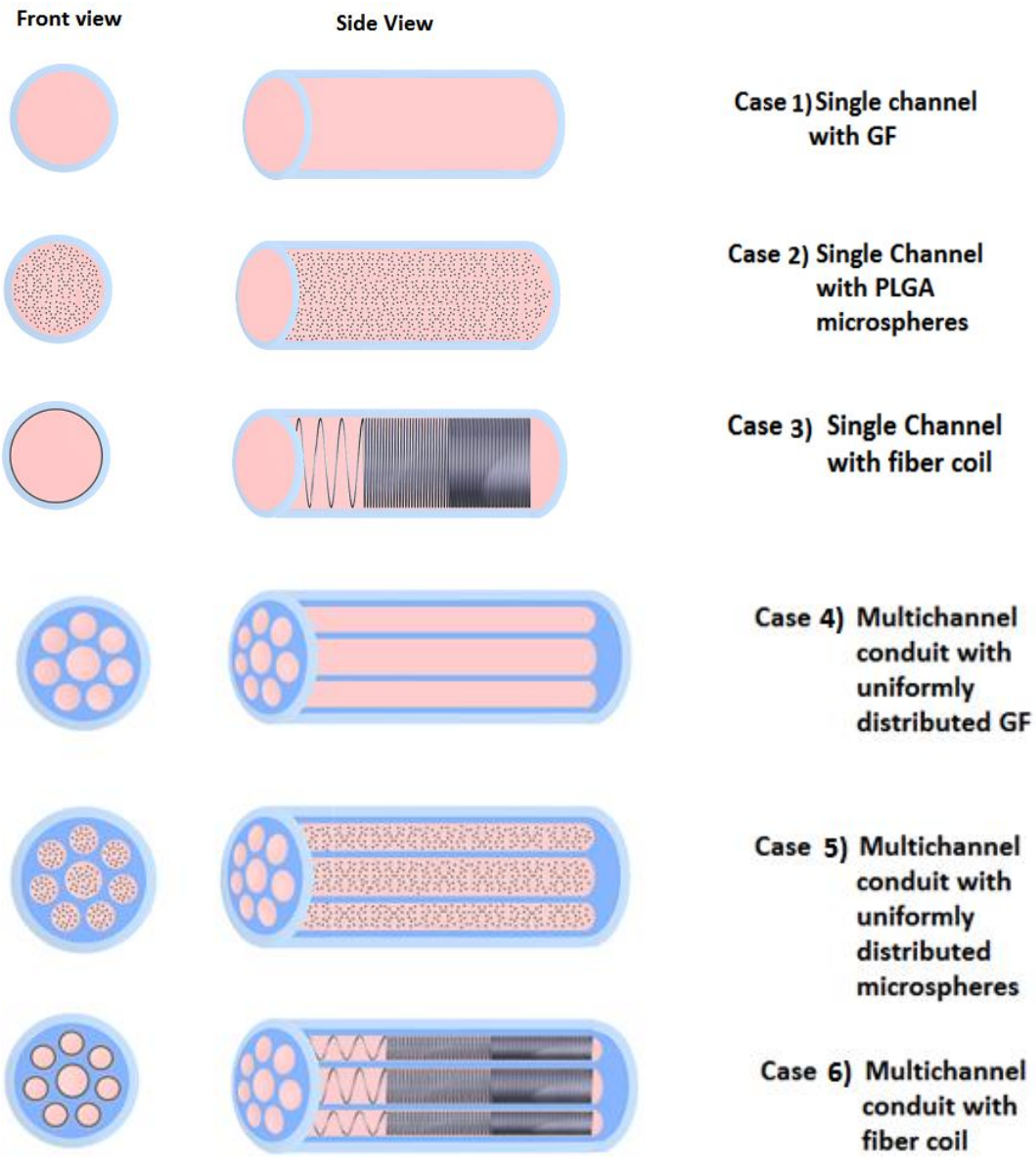

Figure 1-2 Designs of six different nerve guide conduit designs: First three are single channel designs while last three are multichannel variants. Pink color represents collagen while dark blue represents agarose. Light blue represents outer tube enveloping devic

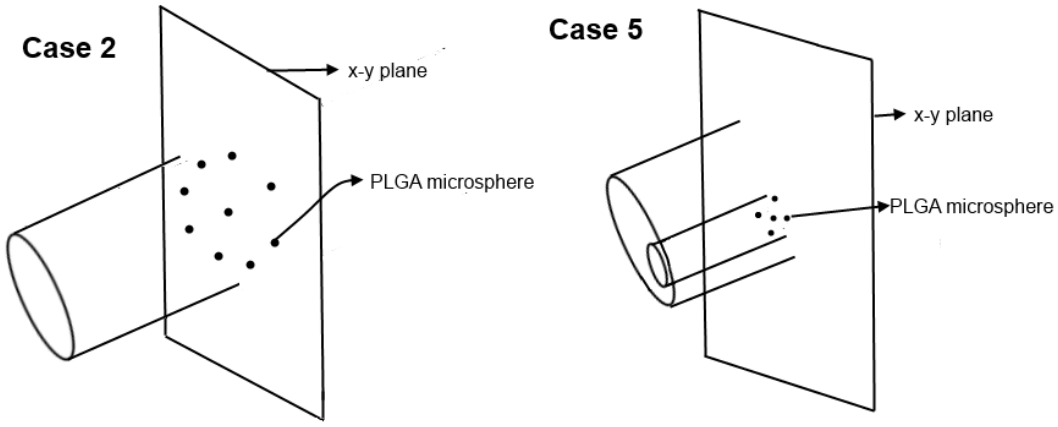

Figure 1-3 Placement of PLGA microspheres in Case 2 and Case 5. For Case 2 the micropsheres are placed in the main channel whereas for Case 5 they are placed in the microchannel.

1.4 Modeling Strategy

Spatio-temporal distribution of drug molecules concentration in a nerve guide conduit following their release can be described by diffusion equation, also known as Fick's second law[17] written as equation 1.

$$\frac{\partial c}{\partial t} = \nabla.(D\nabla c) + R \quad (1)$$

where *c* represents the concentration, *t* the time, *D* the diffusivity of drug molecules, and *R* accounts for the rate of release of species *c* from either drug-loaded microsphere or from the drug eluting stent fibers. We shall apply it to examine the spatio-temporal variations in drug concentration in the NGCs for Case 1-6.

The release term R for PLGA microsphere and drug eluting coil is calculated based on the release data obtained experimentally (section 2.3).Case 1 and 4 can be treated as a simple 1D problem where analytical solutions exist. For other cases, with complicated geometries of the NGC devices, including microspheres and fibers of varying

pitches, a full 3D model is needed and the governing diffusion equations have to be solved by numerical methods, e.g. finite element method. In this project, we develop computational models to compare the drug concentration for all six different cases. Computational models were developed and solved using COMSOL Multi-Physics 4.2 (COMSOL, Inc.).

The general protocol followed is summarized in Figure 1-4. After finding the time course of released GF inside NGC lumen, we further processed these data to interpret the extensional growth of axon in the microenvironment. This post-processing analysis was done using Microsoft Excel (Microsoft).

Since we have different cases that have different geometrical parameters, we define these variables in the software so they can be calculated automatically. The different variables defined in COMSOL are shown in Table 1.1.

Some assumptions need to be introduced for the development of the models. For example, the surface and bulk erosion were ignored for modeling the behavior of biodegradable materials such as collagen substrate and drug eluting fiber coils. In actuality, the erosion and degradation of the substrate are likely to affect the diffusivity of drug molecules in it[11]. For simplicity and to avoid unnecessary excessive computational load, we assume the diffusivity to be isotropic and constant. The degradation of drug eluting fiber could also affect the drug release mechanism, since the average molecular weight of polymer decreases[12]. In this work, we by-passed these concerns since we used diffusivity constants derived from fitting actual experimental degradation data.

Table 1-1: Geometrical variables that are defined in COMSOL

Parameter	Value	Description
r_tube	0.875 mm	Radius of main device
r_microchannel	125 um	Radius of microchannel
r_sphere	2.5 um	Radius of PLGA microsphere
r_coil	50 um	Radius of drug eluting coil
L	10 mm	Length of channel or microchannel
v_tube	$\pi(r\_tube)^2L$	Volume of device
v_microchannel	$\pi(r\_microchannel)^2L$	Volume of microchannel
t1	4	Number of coil turns in first coil zone
t2	27	Number of coil turns in second zone
t3	47	Number of coil turns in third zone
p1	0.72 mm	Pitch of coil in first zone
p2	0.132 mm	Pitch of coil in second zone
p3	0.07 mm	Pitch of coil in third zone
l_coil_single	$2\pi(r\_tube)(t1+t2+t3)$	Total Length of coil in single channel
l_coil_multi	$2\pi(r\_microchannel)(t1+t2+t3)$	Total length of coil in multichannel device
v_coil_single	$\pi(r\_tube)(l\_coil\_single)$	Volume of coil in single channel device
v_coil_multi	$\pi(r\_microchannel)(l\_coil\_multi)$	Volume of coil in multichannel device

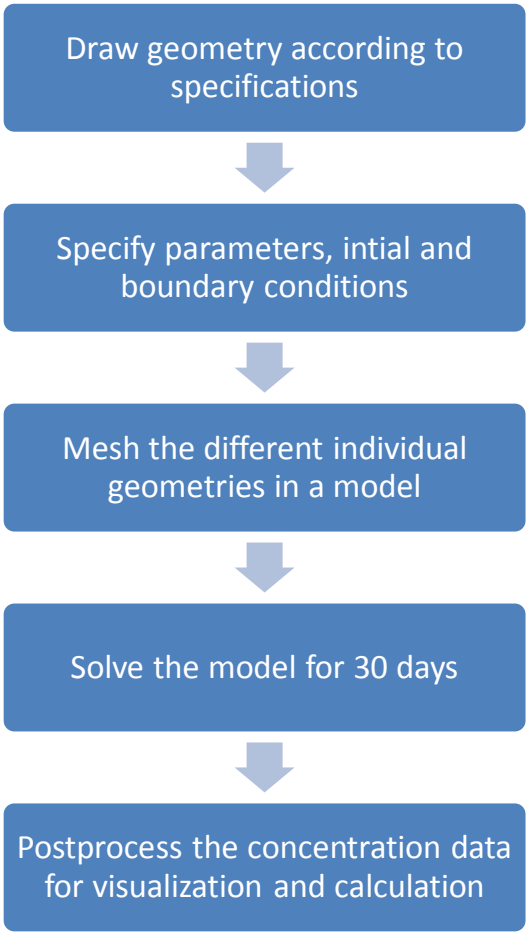

Figure 1-4 Modeling and solving protocol followed for every model

1.5 Thesis Goals And Outline

The primary goal of this work is to examine the diffusion release of drug molecules in NGC device of different designs using computational modeling approach. Computational modeling allows us to predict how the drug concentrations vary inside the channels and how they could affect and guide axonal growth. Furthermore, modeling

predictions could help us to better interpret experimental results, and to refine, optimize channel designs for improved functional recovery and therapeutic outcomes.

Spatio-temporal variation in drug concentration is one part of the project. The study is further extended to develop a protocol that could be used for various models to estimate how straight axons would grow. It is a technique that has allowed quantifying axon straightness. Particle tracing itself is an outcome of processing the spatiotemporal concentration. The idea is based on the fact that axons are attracted and grow towards positive chemotactic gradients provided by neurotrophins such as NGF and repelled by negative regulators[32] (Figure 1-5). Co-ordinate data obtained from particle trajectories is then in turn used to quantify the axon straightness. The quantification method described in this project could very well be applied to experimental data too. For example, if 3D CAD model is reconstructed from confocal image stack, co-ordinates of axon could be extracted and axon straightness evaluated.

Additionally, a preliminary method for drug uptake from axon growth cones using receptor-ligand kinetics has been included. Understanding the kinetics of growth factor binding allows estimation for the consumption rate of the drug, which can then be incorporated into the diffusion models through the consumption term Q_c. An axonal growth model is also described, the physics of which can be included future diffusion models. Major steps of this project are summarized in Figure 1-6.

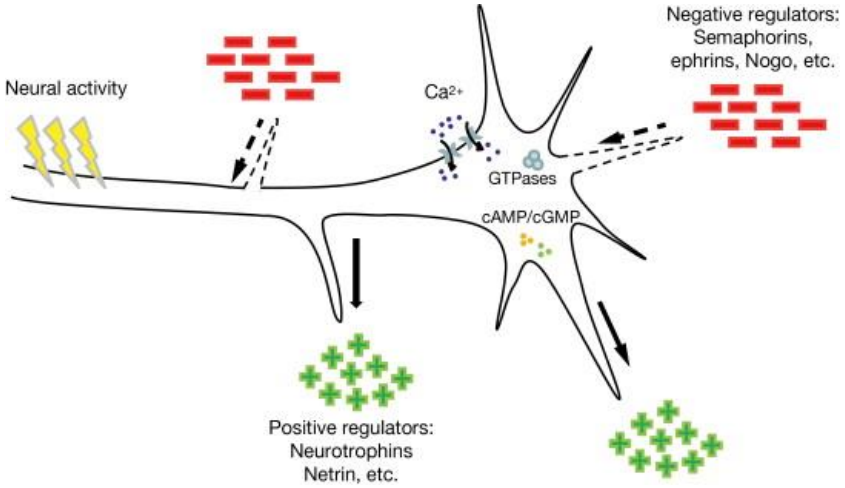

Figure 1-5 The effect of positive and negative stimulus on the directional growth of axon growth cones. Green molecules are attractants while red molecules represent repellants. (From Ref [32])

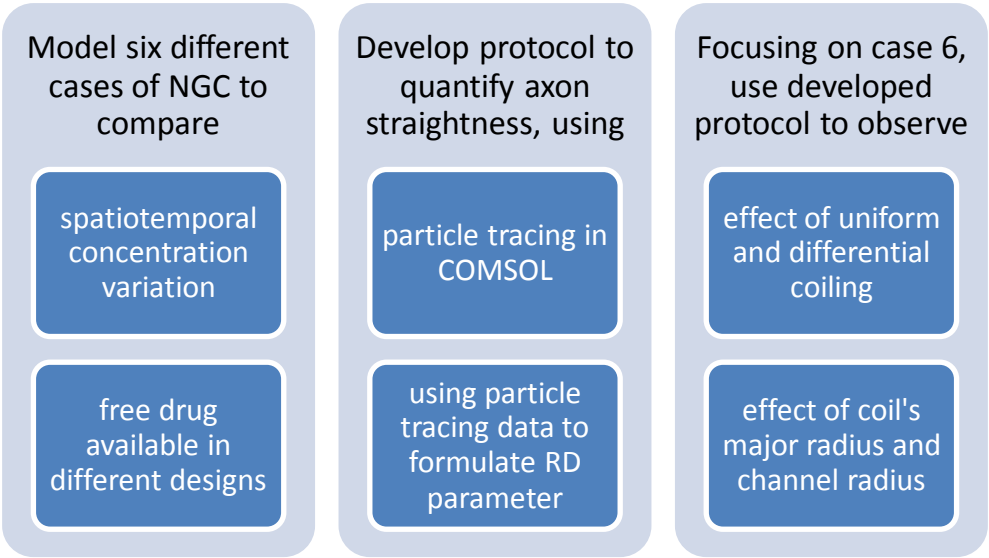

Figure 1-6 Major steps for this project.

Chapter 2

Physics of device

2.1 Designing of device

Drug release to NGC could be accomplished in three different ways: (1) by incorporating the growth factor in conduit filler (hydrogel)[13], (2) by controlled drug release system such as PLGA microsphere or drug eluting fiber, (3) by immobilizing factors into the scaffold[14]. The key point is to maintain a controlled release. Specifically, in Case 3 and 6, axial gradients that continue guiding nerve growth to distal end.

All six cases use a common collagen substrate with same growth factor released to the growing neuron in different ways. Computational simulations allow an in-depth evaluation of different factors that could affect axonal growth. Further, such simulations might reveal any flaws in design that could then be addressed for improvement. Computer simulation can be a powerful tool particularly when multiple growth factors are used in the device. For example, the effect of semaphorin3A known to repel axons[15], can be simultaneously along with NGF to properly direct the axons towards the distal end.

2.1.1 Modeling Details

To simulate the diffusion of drug at either ends of the device, buffers zones were attached with same growth factor diffusivity as collagen. These added buffers allow for natural diffusion at either ends of NGC resembling that in biological system. Furthermore, if the rate of consumption of drug by axons is known, proximal buffer can mimic the effect of growing nerve end (assuming suitable physics are defined). Filler in every microchannel (Case 4, 5, 6) is collagen-based and surrounding media is agarose (Figure 2-1).

For multichannel designs (Case 4, 5, 6), only one channel was modeled with the assumption that event in each of the seven channels is alike and that any diffusion of growth factors to and from neighbouring channels can be neglected because of lack of inter-channel radial concentration gradients. Parameters for all six cases including the method of drug release and amounts used are summarized in Table 2.1; whereas the diffusivities of NGF in collagen and agarose are given in Table 2.2.

Table 2-1 Description of six different cases

Case	Channel diameter	Microsphere		Eluting stent		Axial length (mm)	Amount of drug, M_t (ng) = 100 [ng/ml] x$V_{channel}$	Drug release by
		#	diameter	Fiber diameter	# of turns			
1	1.75 mm					10	2.4	Homogenously distributed
2	1.75 mm	63	5 µm			10	2.4 (0.0381 per microsphere)	PLGA microspheres
3	1.75 mm			50 µm	4/27/47	10	2.4	Drug eluting coils
4	250 µm					10	0.049	Homogenously distributed
5	250 µm	35	5 µm			10	0.049 (1.4E-3 per microsphere)	PLGA microspheres
6	250 µm			50 µm	4/27/47	10	0.049	Drug eluting coils

Table 2-2 Diffusivity of collagen and agarose

Parameter	Value	Description	Source
$D_{collagen}$	7.6×10^{-12} m^2/s	Diffusivity of drug molecules in collagen	Ref 37
$D_{agarose}$	2.3×10^{-14} m^2/s	Diffusivity of drug molecules in agarose	Ref 37

Method for calculating of diffusivities can be found in appendix A. All model geometry was built using the COMSOL module itself. Figure 2-1 shows six modeled geometries.

All the models are based on a 100 ng/ml reference value. This means that the amount of drug used in every channel is the amount that would be required to create a 100ng/ml concentration in that channel. In Case 1 and 4, this amount is simply embedded into the collagen substrate. For Case 2 and 5, the amount is distributed equally among each of microspheres. For Case 3 and 6, the amount is distributed uniformly in the coils.

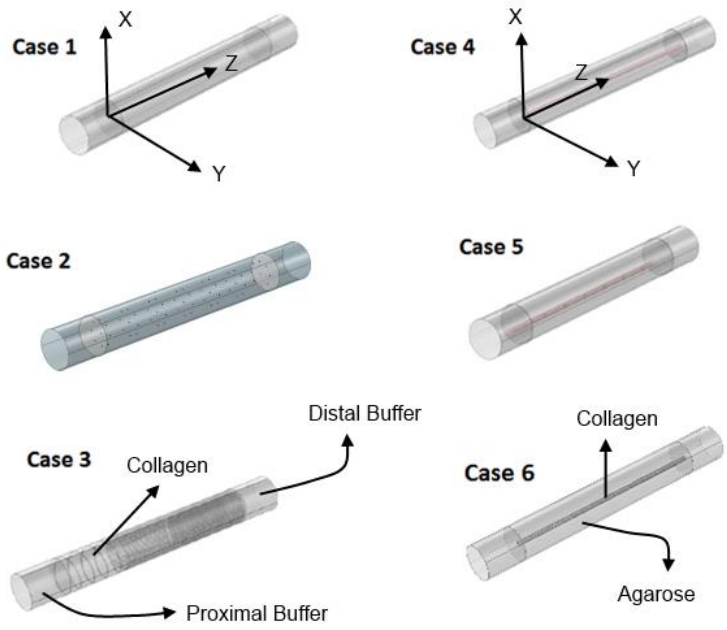

Figure 2-1 Geometries of six models made in COMSOL Multiphysics. For Case 1,2,3 the channel as well as buffers are made of collagen, whereas in Case 4,5,6 the microchannels are filled with collagen and surrounded by agarose.

M_t is calculated by multiplying 100 ng/ml concentration with the volume of channel being modeled ($v_{channel}$). The z axis is the tube's axis in every case, whether it's a single channel device or multichannel one. Z=0 was chosen to be the center of the cross-section of NGC device at its proximal end.

2.1.2 Meshing

The next step in modeling is meshing, which has to be done carefully and individually for every model. Most often, when dealing with controlled drug release materials, there is an initial burst into the surrounding media[16]. Because of this sudden burst, the meshing has to be fine enough to accommodate the high concentration variation around the release source. At the same time, due to computation limitations there is only a certain limit to which mesh can be refined.

Meshing for Case 1, 4 were done relatively easily since the size of all the involved geometries is big enough to allow easy meshing. All the other cases on other hand have volumetric drug releasing sources which are very small compared to total size of geometries. As a result, meshing had to be done repeatedly with different refinements for the COMSOL solver be able to solve it correctly. For coilconfiguration, the coil was broken down into three individual parts and meshed separately. Tetrahedral elements were used for all geometries in this project. Other type of elements such as brick, prism and pyramid (Figure 2-2) can also be used but they have to be used carefully and only if needed. The main motivation of using brick and prism elements is that they can help reduce the total number of mesh elements in the model (see Appendix B). Bricks and prism are also preferred choice if we know that the solution varies slowly in one or more of the directions. In our case, we have a very fast release from coil during initial times,

and therefore went very fine tetrahedral volume elements for coil as well for surrounding medium.

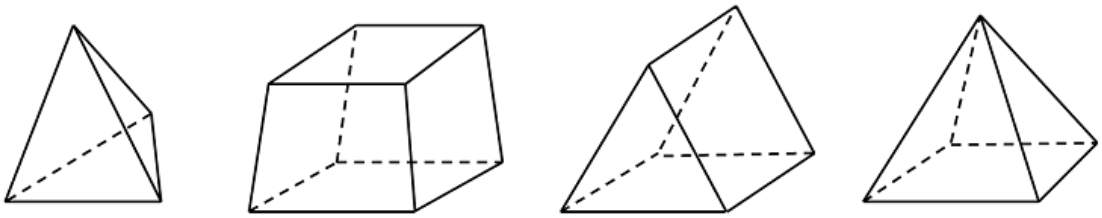

Figure 2-2 Four different types of element commonly used in finite element models: tetrahedral, brick, prism and pyramid elements.

Regardless of the type of elements used, it is usually wise to change mesh sizes and observe if solution changes. And same protocol was adopted for all models. Initially, to see the difference in element sizes, a variant of Case 1 was modeled with a large minimum element size. We assumed a situation where there are no buffers and that either ends of channel are maintained at 0 ng/ml concentration. Since this case can be solved analytically we can observe the effect of numerical solutions converging to exact solution as we refine the element mesh sizes.

Although, the above mentioned validation method can only work with Case 1, since there is no analytical solution for other cases. Other models were solved for different element sizes and a minimum element size of 1 um for PLGA microspheres and 8 um for coil were fixed. The final meshes for the geometries are shown in Figure 2-3.

The coils were modeled as three separate entities. This was done because the coiling does not follow an equation for pitch; the change is discrete. There are three zones of coiling: low turns (4), medium turns (27) and high turns (47). Separate modeling of coils was apparently also beneficial for meshing. COMSOL Multiphysics often presents with difficulties when meshing helical geometries and they have to be broken up in parts.

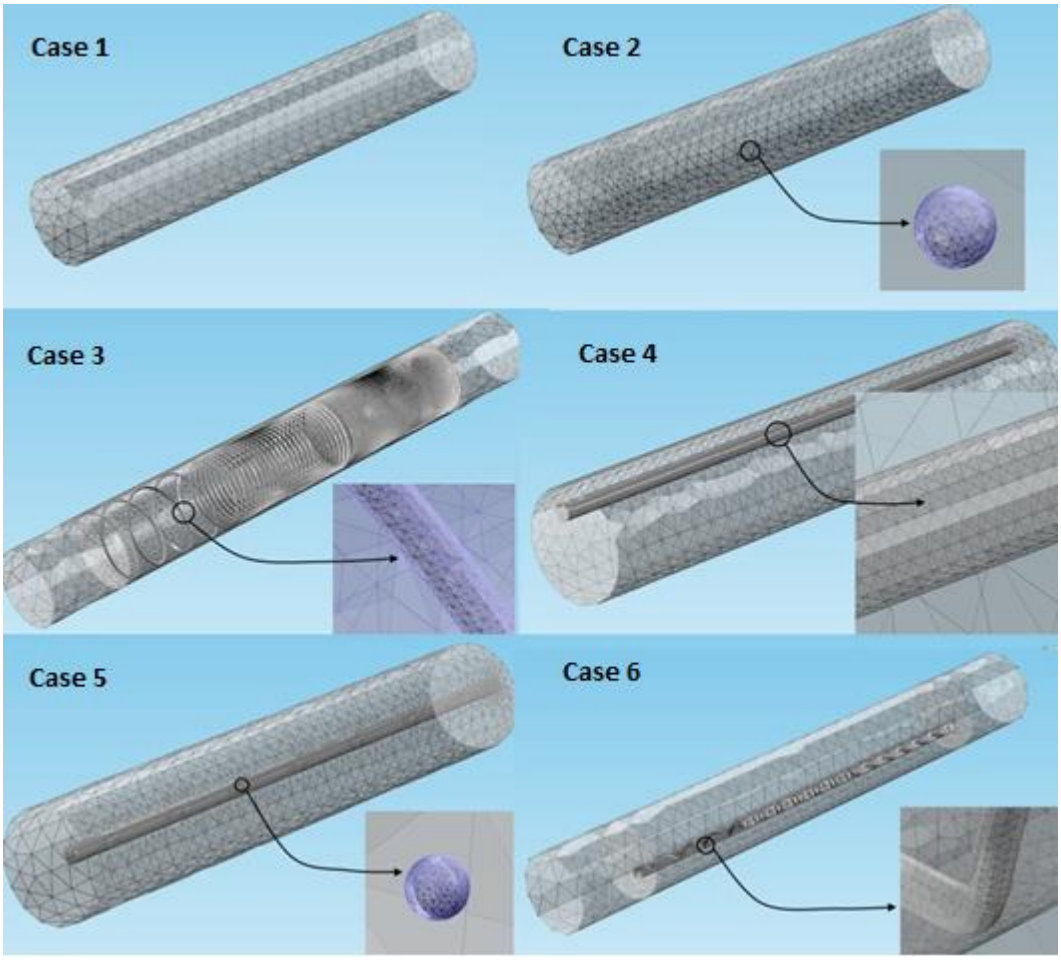

Figure 2-3 Meshed geometries depicting the different size of mesh elements. The critical geometry parts are zoomed in separately because of the scale difference.

The diffusion equation governing the release of drugs within the NGC can be written as equation 2.

$$\frac{\partial \mathrm{c}}{\partial \mathrm{t}} = \nabla.(\mathrm{D}\nabla \mathrm{c}) + \mathrm{R} + Q_c \qquad (2)$$

where c is the concentration of the drug (ng/ml), ‘t’ is time (seconds)

R represents the rate of release of drug per unit volume from the PLGA microspheres or drug eluting fiber (ng ml^{-1} s^{-1}), and Q_c represents the rate of consumption of the species. The Q_c term will be explained in more detail in section 2.6 on the discussion of receptor-ligand kinetics.

Drug release in NGC for a variant of Case 1 was obtained from analytical solution. As an example for FEM calculation, it was solved using COMSOL as well and the numerical solution were compared to that from analytical solution. We assume the growth factor is uniformly distributed inside lumen and ignore material degradation. We also ignore the buffers for this sample calculation and assume no flux on all boundaries. Then model can be assumed to be a 1D model since concentration varies only in the axial direction. Equation 2 then can be solved analytically as follows.

Assume the axial direction is the z axis. A plane x-z is considered for calculations Then the domain of interest would be a rectangle; over which the equation is solved. Next we simplify this rectangle to just a straight line since concentration will vary only along the axial direction (Figure 2-4(A)). We also assume there is no consumption rate Q_c or production rate R. Equation 2 then can be simply written as equation 3.

$$\frac{\partial \mathrm{c}}{\partial \mathrm{t}} = \mathrm{D}\frac{\partial^2 \mathrm{c}}{\partial^2 \mathrm{z}} \tag{3}$$

where z varies from 0 to 10 mm. Using separation of variables, equation 3 can be solved for c with solution expressed as equations 4 and 5[40].

$$C(z,t) = \sum_{n=1}^{\infty} B_n \sin\left(\frac{n\pi z}{L}\right) e^{\frac{-Dt(n\pi)^2}{L^2}} \tag{4}$$

where

$$B_n = \frac{2}{L}\int_0^L C_i \sin\left(\frac{n\pi z}{L}\right) dz \tag{5}$$

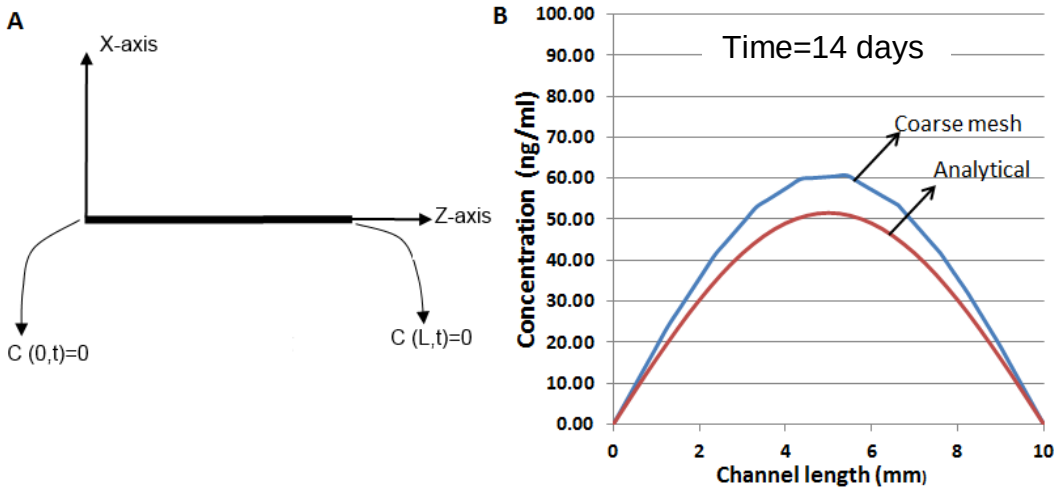

Figure 2-4 A) The rectangular cross-section of channel can be assumed as 1-D with either ends at 0 ng/ml. B) Plot showing the error in concentration that coarse meshing can have.

Considering boundary condition at proximal and distal ends written as c (0, t) =0 and c (L, t) =0, spatiotemporal concentration changes in NGC were calculated for 14 days. Assuming initial concentration in channel C_i = 100 ng/ml, we compare the concentration variation obtained from coarse meshed computer model with analytical solution. The 3D meshed model had a total of 270 tetrahedral elements. Coarse meshing leads to an increased concentration with a peak error of 14.7% occurring at center of channel.

2.2 Drug Release Kinetics

Release kinetics can either be based on a mathematical model or on experimental data. Here, we formulate release rate equations based on data obtained from experimental drug release data. Power law equation is utilized to define the

fractional drug release from the microsphere and coil, and in general form is given by equation 6. K and n are constants that are obtained by experimental data.

$$f = Kt^n \quad (6)$$

where K (0.37) and n (0.25) are constants which characterize the drug release[37]. The release profile is shown in Figure 2-5 where the values had been obtained by fitting the PLGA microsphere release data over a time period of 30 days.

The drug release profile from the drug eluting coil is estimated from release data of first 250 hours obtained from the manufacturer (TissueGen Inc, Dallas, Tx). The fractional release profile for drug eluting coil is shown in Figure 2-6. Logarithm of values was taken and fitted in an equation of form y=mx+c. The calculations yield values of K=0.61 and n=0.088 for the release kinetics equation $f=K*t^n$ .The data is extrapolated in our simulations till 30 days.

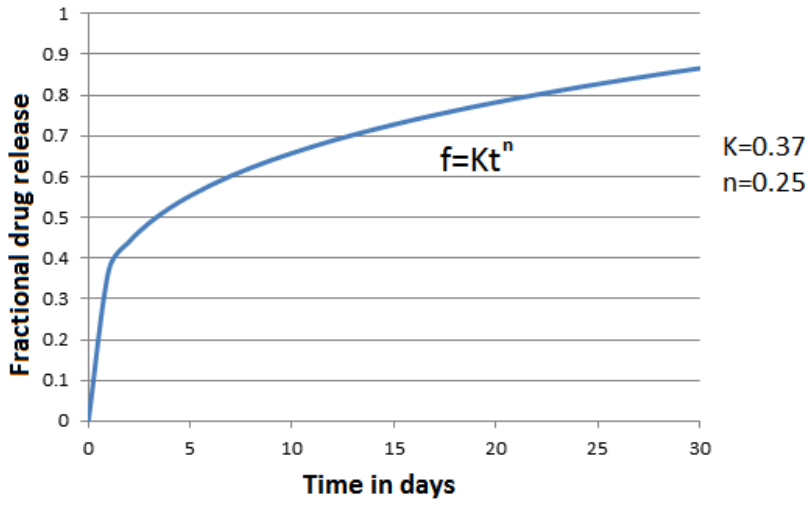

Figure 2-5 Fractional drug release profile from a 5 um PLGA microsphere over 30 days.

It is clear from the coil drug release profile (Figure 2-6) that there is a very sharp initial burst. Around 60% of drug is released within an hour. This has a significant effect in the computer simulations simply because of the range of difference in timescales. The mesh around the drug eluting fiber in the computer model has to be extremely fine to accommodate this burst.

Because of the nature of computer modeling, we are interested in the rate of drug release rather than fractional drug release. To calculate the rate of release, the equation for fractional drug release was differentiated with respect to time yielding, equation 7 and 8 for microsphere and coil.

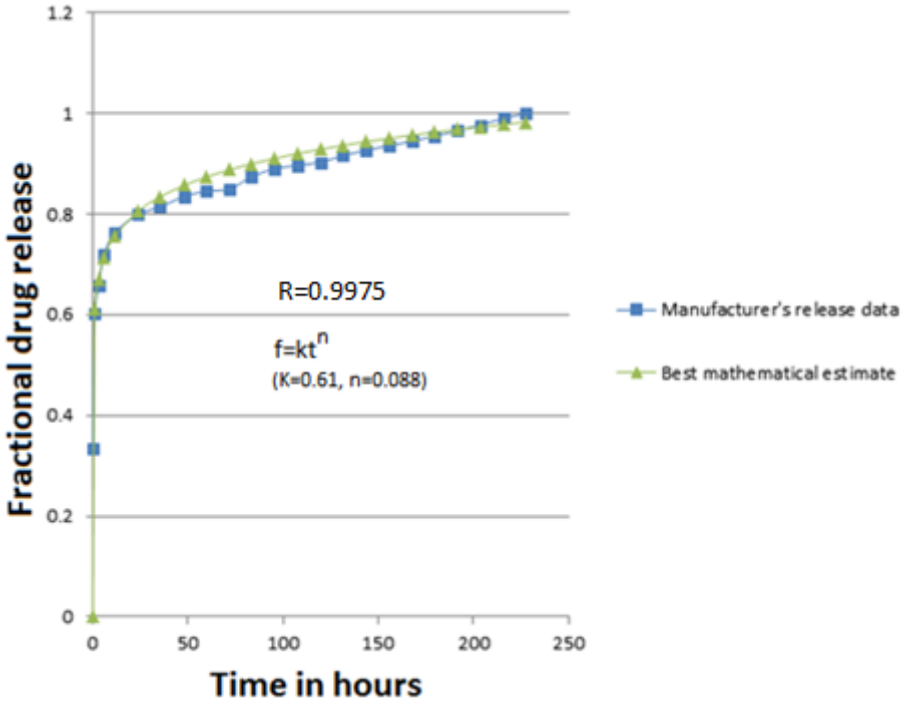

Figure 2-6 Drug release profile is obtained and recorded experimentally for first 250 hours and then fitted mathematically where the R-value means correlation coefficient.

$$\frac{df_{microsphere}}{dt} = 0.0925t^{-0.75} \quad (7)$$

$$\frac{df_{coil}}{dt} = (0.0536)(t^{-0.912}) \quad (8)$$

Fractional release rates are shown in Figure 2-7 Note that the release rates reach infinity as time approaches zero for both equation 7 and 8. Piecewise function was used for their incorporation to avoid mathematical singularity when solving of diffusion equation 3.

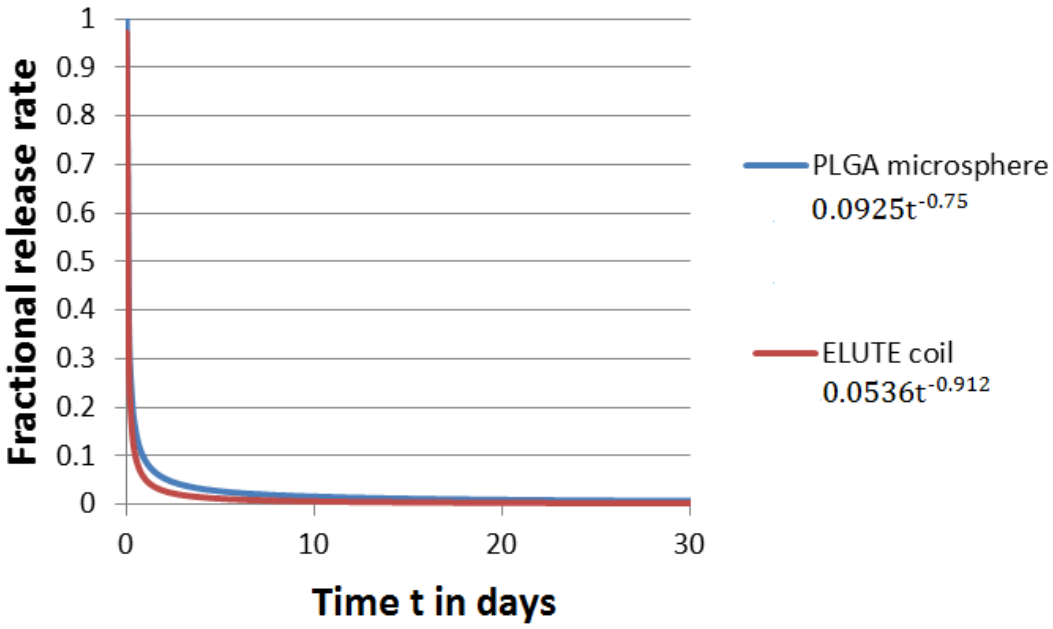

Figure 2-7 Fractional release rate profiles for PLGA microsphere and drug eluting ELUTE coil. For time<1 hr, the fractional release rate is assumed constant to avoid division by zero value.

For PLGA microsphere

$$reac_{microsphere}(t) = \begin{cases} 1.0029, & t < 1hr \\ 0.0925t^{-0.75}, & t \geq 1hr \end{cases} \quad (9)$$

For drug eluting coil

$$\mathrm{reac}_{\mathrm{coil}}(\mathrm{t}) = \begin{cases} 0.972, & \mathrm{t} < 1\mathrm{hr} \\ 0.0536\mathrm{t}^{-0.912}, & \mathrm{t} \geq 1\mathrm{hr} \end{cases} \quad (10)$$

Equation 9 and 10 are still fractional release rates which need to be converted to volumetric release sources with the multiplication of (M_t/V_{source}); where M_t is the total amount of drug used in the channel and V_{source} is the volume of release source. We calculate M_t based on different cases. M_t would be the amount of drug needed to create a 100 ng/ml concentration in the NGC channel. V_{source} represents the volume of source, which can either be PLGA microsphere or coil. Using this methodology we can assign a volumetric drug release source term, in individual cases. All the terms were calculated and adjusted prior to their use in the FEM model.

2.3 Particle Tracing

To be able to visualize the probable path, that an growing axon from nerve stump would take, we compute particle trajectories inside the lumen. The idea is to release particle(s) from the proximal end from where the axons grow. These particles are massless and are given the property to sense net chemotactic gradient vector in the space. Therefore, in the presence of an external concentration field which is obtained after solving a model, the particle will follow the vector path. The final gradient vector is the sum of individual vector gradients in x,y and z direction calculated at each data point (equation 11). Then, the direction of final vector (Grad c) is what the particle traverses (Figure 2-8). The magnitude of the vector can be assigned in the color coding legend in the software for interpretation.

$$Grad\ c = \frac{\partial c}{\partial x} i + \frac{\partial c}{\partial y} j + \frac{\partial c}{\partial z} k \quad (11)$$

Implementing such technique allows for a very clear picture and understanding concentration differences, as well as differences between different designs. The method is based on a very simple mathematical principle of vector sum, but produces extremely important results. Moreover, the trajectories of these particles themselves allow for the quantification for axon straightness. This method is covered in section 2.5. Therefore, this method serves two purposes:

1) Allowing for visualization of probable axon paths.
2) Providing raw co-ordinate data of the trajectories which can be used for straightness quantification

Implementation of this technique is done in simulation section for different scenarios. This method can be extended by including more physics. This can be done by assigning the particle an mass which would allow it to experience drag forces in the substrate. If a signal-transduction mathematical model can be formulated, then an approximate cytoskeletal pushing force can also be assigned to the particle.

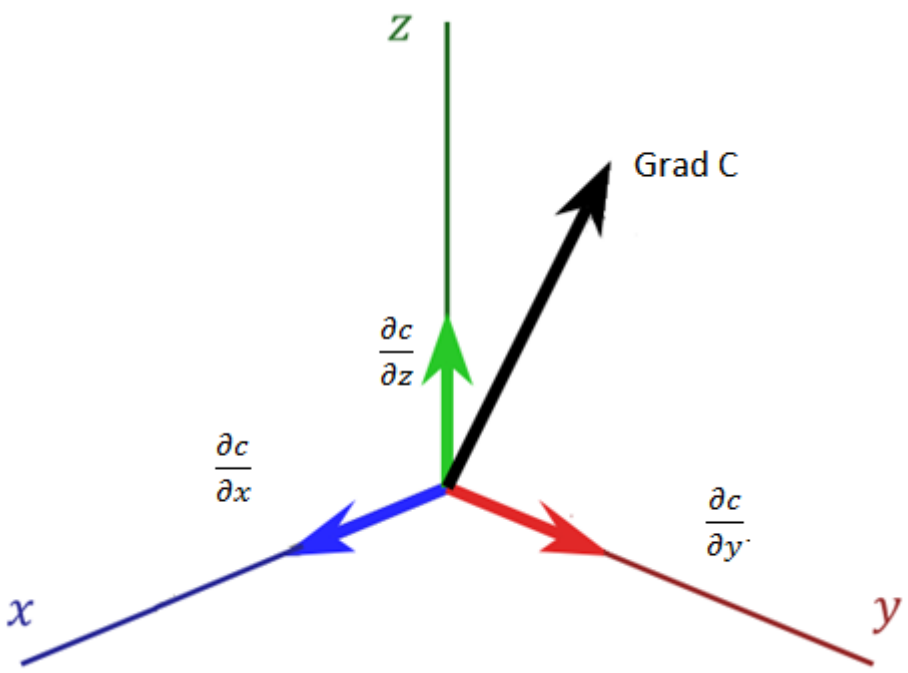

Figure 2-8 Principle of particle tracing showing the sensing mechanism of particle. The vector of individual gradients in x,y and z direction is taken.

Since axon straightness (linear growth) is one of the most important aspects of good NGC design, quantifying it is very essential. This way axonal diversion in NGC can be compared among different designs. The method can also be applied to experimental data if coordinate data can be obtained through 3D reconstruction of the confocal data. Three different ways were initially thought to accomplish this. The method that has been adopted is mentioned below. The other two methods can be seen in appendix C.

2.3.1 Radial Dispersion

The method which was used for quantification was “radial dispersion” measurement, RD. RD essentially represents the radial distance of any point on an axon from a relative axis passing through axon’s starting point. To get an understanding of this

method imagine the following scenario. Let us assume we have the coordinate data (x,y,z) for an axon trajectory growing inside a channel. Then at any point Q(xi,yi,zi) on the axon, the distance from the central axis of lumen will be the radius of circle with Pi as the center. This value will be given by $\sqrt{(xi^2+yi^2)}$. But it is preferred that we shift the central axis to one that passes through the starting point A (x_A,y_A,z_A) of axon. Therefore, now the RD after shifting to the new axis is $\sqrt{((xi-x_A)^2+(yi-y_A)^2)}$. Axis shifting is done so that RD can be compared to other models.

RD gives the estimate of axonal radial dispersion. This parameter also allows getting a rough estimate of how correct the innervation is since incorrect innervation at distal target is often a problem associated with NGCs[24]. The diagrammatic representation of RD calculation is shown in Figure 2-9.

If we have multiple points like (x_1,y_1,z_1), (x_2,y_2,z_2), (x_3,y_3,z_3)…….. (x_n,y_n,z_n), then the net RD will represent the average of individual RD's which can be written as equation 12.

$$\text{Mean RD} = \frac{(\text{RD1+ RD2+ RD3}.....\text{RDn})}{\text{n}}. \quad (12)$$

This way we get an estimate of how much an axon is diverging from its own axis along with the average radial deflection. This method is adopted in the Results section using data from particle tracing.

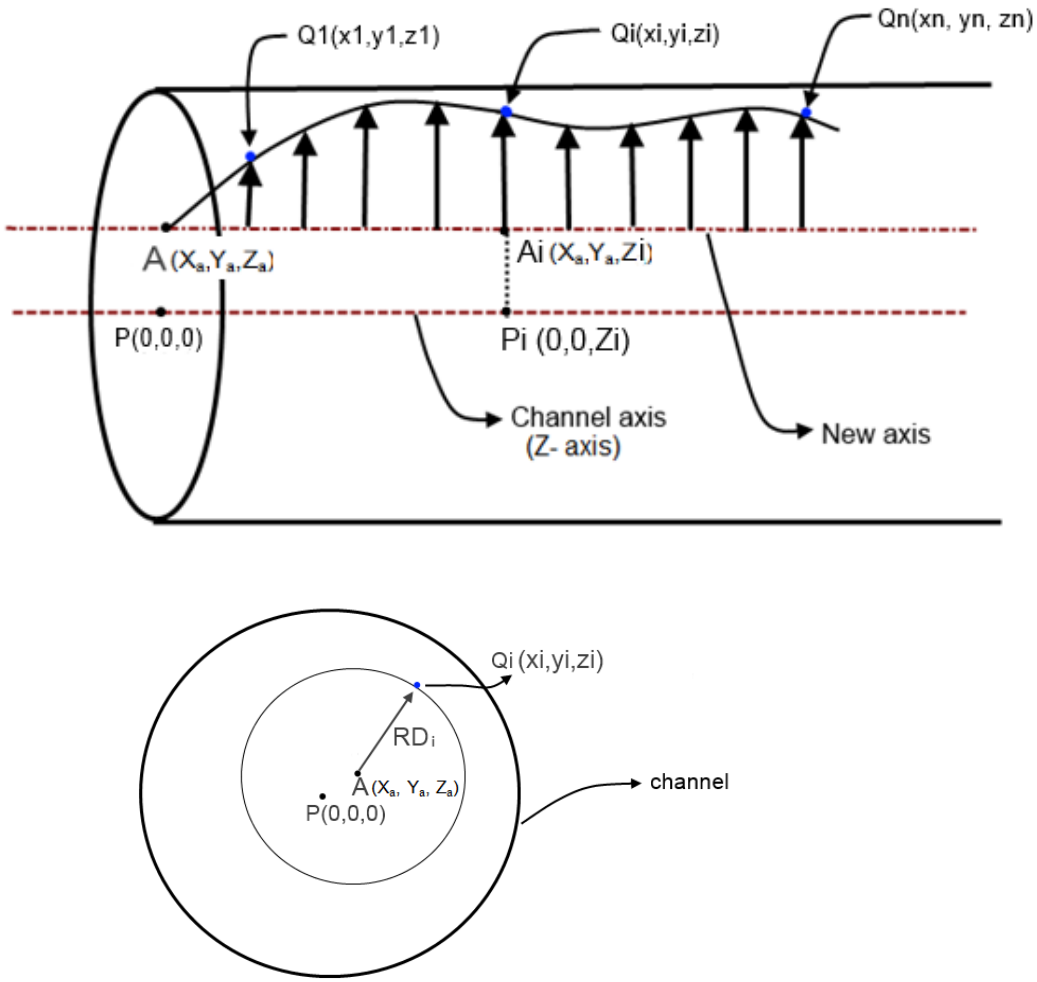

Figure 2-9 Diagram showing the physical interpretation of RD in context of NGC. A) Vertical arrows represent individual RD's at each data point along the axon. B) Cross-section view through a plane passing through Qi and perpendicular to z-axis.

2.4 Receptor Ligand Kinetics

We know that the growth cone consumes the growth factor (NGF) and this leads to the elongation of axon[33]. We try to formulate a preliminary analysis/model for ligand

consumption so that a rate of consumption term Qc can be estimated and used in Fick's law in the computer model.

In the simplest chemical process, a monovalent ligand L binds with a monovalent receptor R to form a receptor-ligand complex C.

$$R + L \leftrightarrow C$$

The forward and backward rate constants for such a reaction are k_{on} and k_{off}.

When talking about axons and ligands binding with it, the site of binding normally is the axon tip/growth cone[25]. In our context, this is called specific binding, i.e. the binding of interest. But since in a natural tissue there are a variety of cells possibly expressing same receptors, there is possibly undesired receptor-ligand activity too. This is called non-specific binding. In the following calculation we ignore any non-specific activity.

There are mainly three ways[26] that NGF can induce signaling cascade. NGF can bind with:

1) P75 low affinity nerve growth factor receptor, p75(NTR)
2) trkA, a transmembrane tyrosine kinase receptor
3) heterodimer of p75(NTR) with trkA, which also has a very strong affinity and specificity to NGF.

Taking a deeper look at the drug delivery system, it can be seen that NGF will exit the main device (tube) in the following ways:

- NGF gets internalized because of binding with a receptor on either an axon growth cone, or any other cell.
- NGF simply diffuses through endoneurium and epineurium (Figure 2-10)

P75(NTR) also binds with other related growth factors such as BDNF, NT-3, NT-4[28] . Although in the devices being modeled only NGF is used as the growth factor.

As we scale down into the structure of axon, we see that receptor-ligand binding gets very complicated. Figure 2-11 briefly explains the chemical kinetics in the stages that happen at an axon growth cone extension[27]. It is clear that there are multiple processes happening at the cellular level.

It is realized that estimating a value for rate of ligand consumption is extremely challenging if all factors such as receptor up-regulation and down-regulation are to be accounted for, since all these parameters are interdependent (see appendix D), and values for many are not known.

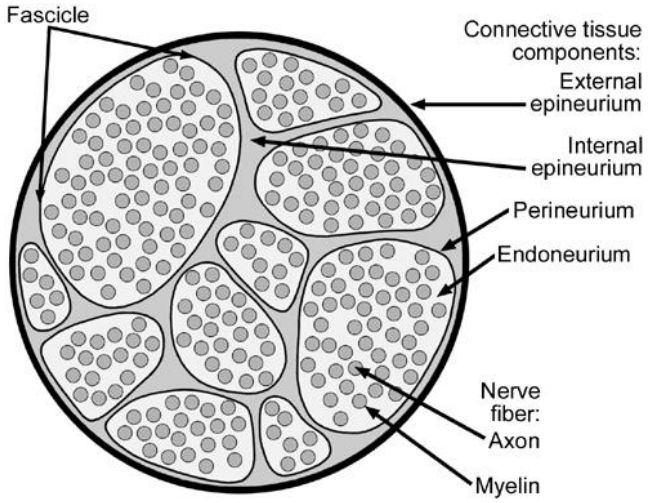

Figure 2-10 Cross-section of a typical peripheral nerve. It can be seen the total surface area is divided between axons, epineurium and endoneurium[38].

Therefore, we proceed with many assumptions mentioned as follows:

1) Both ligand (NGF) and receptor are monovalent, i.e., there is only one binding site on those molecules.
2) We do not differentiate between low affinity (P75) and high affinity (trkA) receptors.

3) Receptor upregulation and downregulation is ignored.

4) NGF binding with p75-trkA heterodimer is also ignored.

5) Only one growth cone is associated per axon

6) We assume the single channel model for calculations.

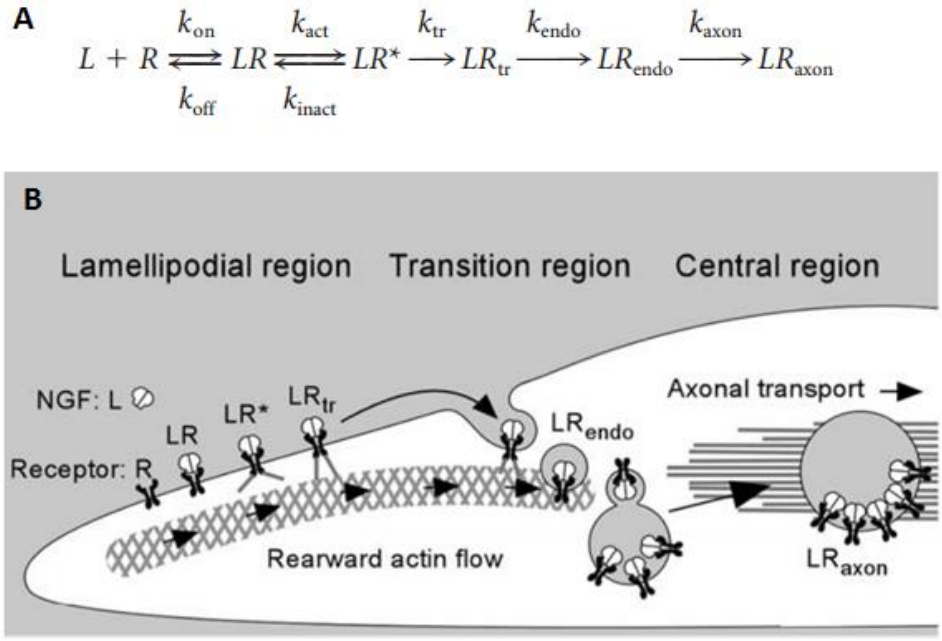

Figure 2-11 Schematic representation A) the chemical kinetics between different stages of binding, and B) NGF internalization process on axon growth cone.

2.4.1 Scaled cell density

At first we want to estimate if the ligand internalization is significant as compared to the overall concentration. For this, we calculate a term “scaled cell density” η (equation 13) which simply means the ratio of total cell receptors to total ligand molecules in system.

$$\eta = \frac{\mathrm{n}R_t}{N_{av}L} \tag{13}$$

where n is the number of NGF receptor-bearing cells per unit volume. R_t is the total number of NGF receptors per cell. N_{av} is the Avagadro's number (6.023E23 mol^{-1}). L is the concentration in M. Parameters used and reference sources are summarized in Table 2.3.

Table 2-3 Different parameters associated with receptor-ligand kinetics

Parameters	Values	Sources
Number of NGF receptors per axon growth cone (R_t)	10^4	Ref 34
Dissociation constant (K_d)	$2x10^{-10}$ M	Ref 35
Endocytic rate (k_e)	$2.5x10^{-3}$ s^{-1}	Ref 26

We assume that there are 27000 axons[10] in the proximal nerve stump for Case 3 (number of axons in a rat sciatic nerve). And that all growth cones (tips of axon) are in a volume represented by a cylindrical disk of thickness 't' at a distance 'a' from the proximal nerve (Figure 2-12).Therefore using these values n can be written as equation 14.

$$\mathrm{n} = \frac{27000}{\pi r^2 t} \tag{14}$$

where r is the radius of the proximal nerve stump (0.875 mm). Therefore, using 0.875 mm for radius, n was calculated to be (1.53E7)/t. η can now be expressed as equation 15.

$$\eta = \frac{2.54X10^{-13}}{Lt} \tag{15}$$

We calculate η for three values of 't' and vary the concentration from 0.0073-0.713 nM (1-100 ng/ml). The variation is shown in Figure 2-13. η varies from 0.19 for high concentrations to 35.6 to low concentrations. Ligand consumption is usually assumed significant if η>0.1[34].

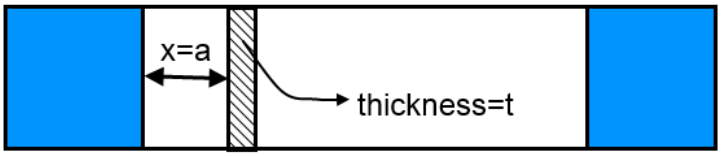

Figure 2-12 Schematic to show the active volume 'V' where most of the receptor ligand binding happens. The shaded region represents the volume 'V'.

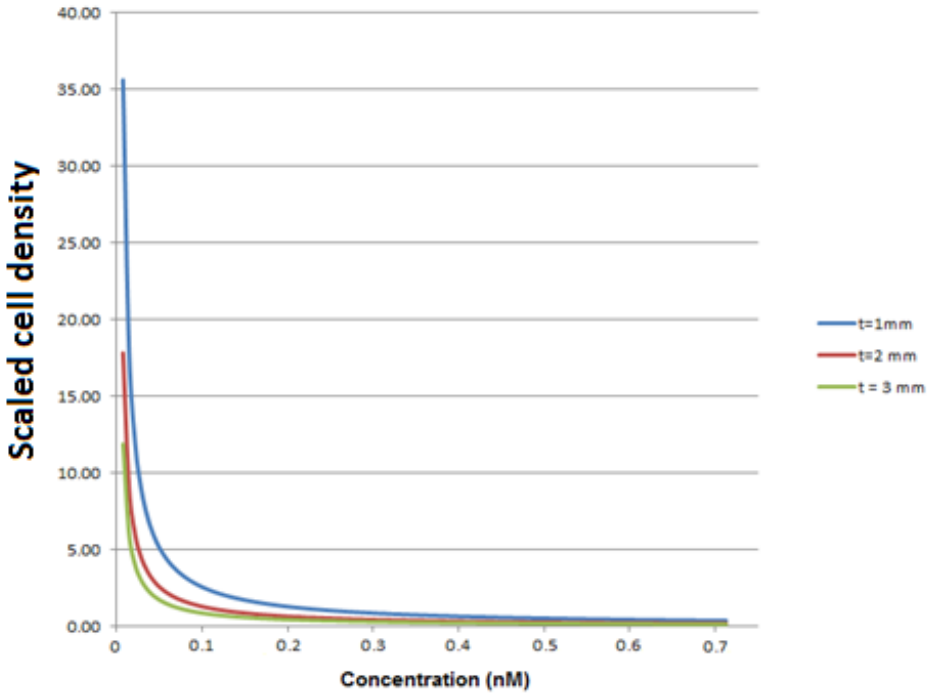

Figure 2-13 Scaled cell fraction vs the concentration (nM). η varies from 0.19 for high concentrations to 35.6 to low concentrations.

2.4.2 Ligand consumption rate

Now that we have established that the effect of ligand consumption is significant we proceed onto estimating that value. Our interest lies with the amount of ligand that gets internalized per unit time. This number will also be equal to the number of complexes that get internalized.

Since L varies inside the device because the active volume 'V' keeps on moving ahead (Figure 2-12), we formulate the rate of consumption in terms of L. At equilibrium the fractional occupancy u_{eq} of receptors is given by[34] equation 16.

$$u_{eq} = \frac{L[1-\eta u_{eq}]}{K_D + L[1-\eta u_{eq}]} \tag{16}$$

The equation is a quadratic equation and yields equation 17 as the solution for u_{eq}.

$$u_{eq} = \frac{-(L+K_d+L\eta)+\sqrt{[(L+K_d+L\eta)^2-4L^2\eta]}}{-2L\eta} \tag{17}$$

where K_d is an average dissociation constant assumed between NGF and NGF receptors. Assuming endocytic rate of K_{endo} s^{-1}, the rate of internalization of these occupied receptors is $u_{eq}K_{endo}$ molecules s^{-1}. This will also be equal to the number of ligand molecules consumed since they are bonded to receptors.

The volumetric rate of ligand internalization in M s^{-1} can then be written as equation 18.

$$Q_c = \frac{k_{endo}u_{eq}}{10^3 V N_{av}} \tag{18}$$

We can specify this consumption term Q_c in COMSOL for a cylindrical disk at the proximal end. Although, in the computer model this disk is stationary and does not move ahead with respect to time.

NOTE: Generally, ligand consumption studies are done in culture experiments and ‘V’ is the volume of liquid media in which the cells are uniformly present. The values of different parameters such as endocytic rate are also based on such studies. It is not known whether the behavior of axon growth cone in a 3D scaffold is same as in an almost 2D culture plate. It is possible that there might be significant difference since the mechanical properties of scaffold also play a role. Furthermore, more surface area of axon growth cone is exposed to growth factor in 3D than in 2D.

Chapter 3

Simulation and Results

3.1 Simulation Overview

Total of 6 different models were modeled as explained in chapter 1. But most of post processing emphasis is on models with coil configurations. All the simulations were carried out for 30 days. For comparison of the six models, the amount of drug used in each modeled channel was equivalent to the amount that would create a 100ng/ml concentration in the active channel.

A common protocol that is followed in the following sections is to measure axon straightness by using particle tracing that has been mentioned earlier. Figure 3-1 briefly explains the protocol for quantifying axon straightness.

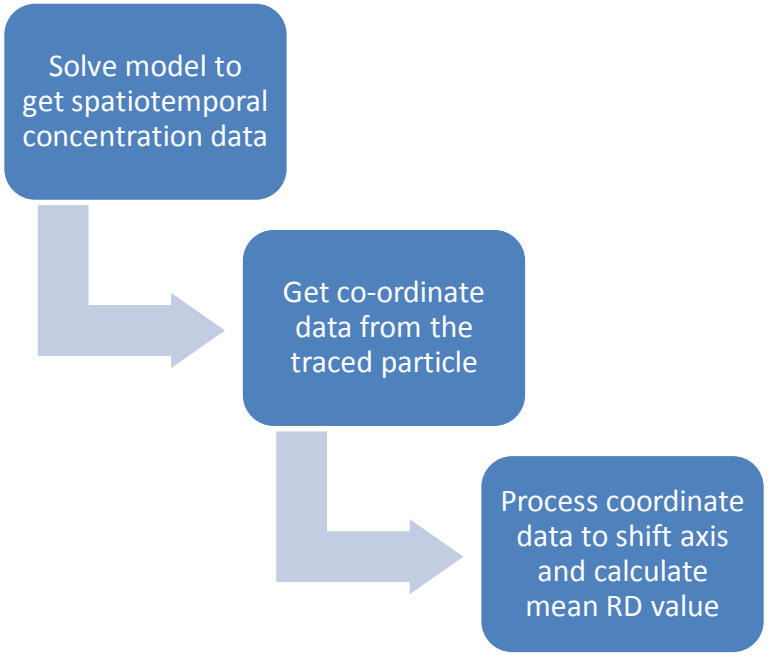

Figure 3-1 Illustration showing protocol to measure axon straightness.

3.1.1 Assumptions and Boundary Conditions

- Before moving to simulation and results it should be noted that there are certain assumptions that have been made for all models:
- The collagen based scaffold and the drug eluting fiber do not degrade in the simulations; and diffusivity remains constant.
- Consumption of drug via axons is not considered the simulations.Proximal nerve stump is assumed to be stationary.

The boundary conditions for all six designs are shown in Figure 3-2. The two cylindrical buffers on either side act like surrounding tissue to which the drug can diffuse through from the device.

No flux boundary condition is assigned to all outer boundaries of all models. The initial concentration in both buffers as well as channel is assigned as zero. The initial concentration for micropshere or coil is calculated according to the variables defined in COMSOL. For microsphere the initial concentration will be given as M_t/v_sphere where M_t is the amount of drug per microsphere. For coil, the initial concentration will be given as M_t/v_coil. In the latter case Mt represents the amount of drug in coil.

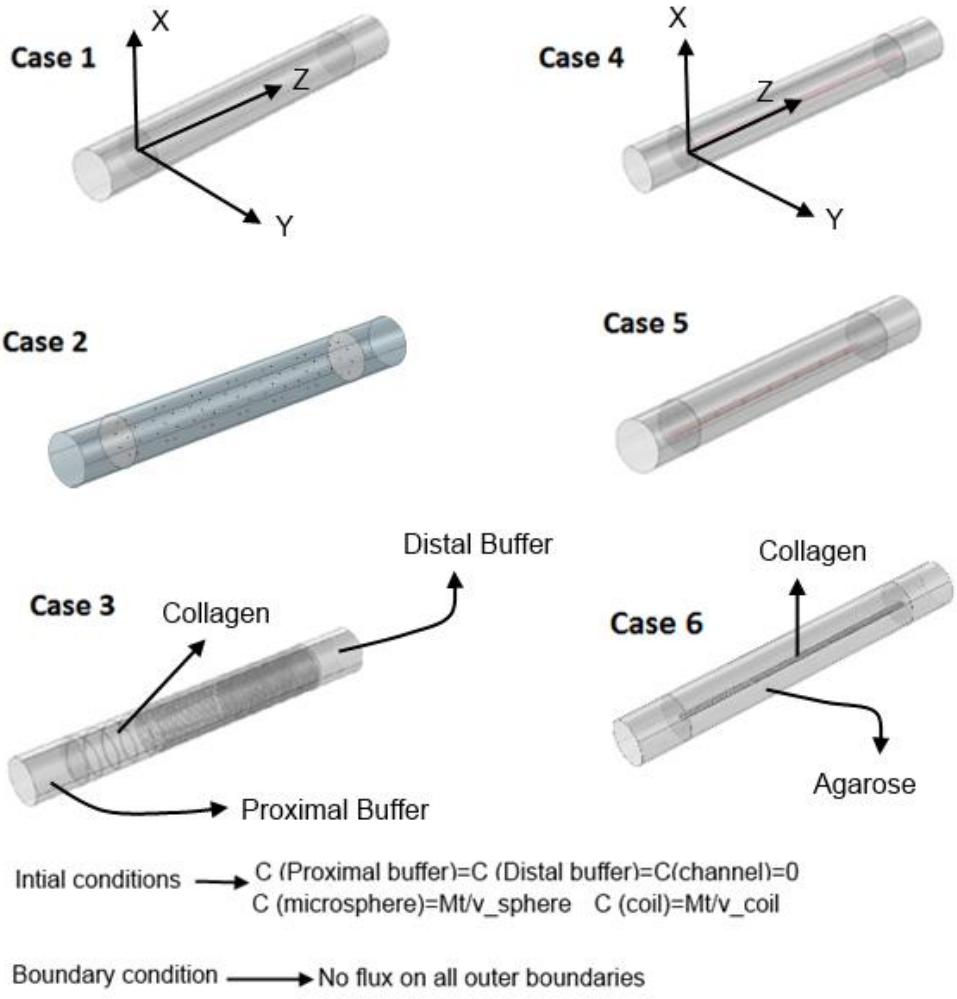

Figure 3-2 Boundary conditions (BC's) that are applied to the six models. The BC's are same for all models: 0 flux on all outer surfaces, and the buffers at 0 initial concentrations. The initial concentration for microsphere and coil are calculated according to COMSOL defined variables

3.2 Results of Six Designs

The first step in understanding concentration variations in different designs is to compare the transient axial concentration changes in all designs. All the simulation studies were done for 30 days with similar boundary conditions. The results of the

simulation are shown in Figure 3-3. Scaled up version for Case 4 and 5 are shown in Figure 3-4. The different time points that were considered are 1, 2,3,4,5,10,20,30 days.

In a nerve regenerative conduit, two things are desired:

1. Sustained presence of growth factor inside the active lumen
2. Continuous presence of a positive chemotactic gradient along the axial direction.

Out of these six designs, it can be seen that while Case 1, provides a high amount of drug presence (average 80.59 ng/ml), the gradient is only present for the first half of the lumen, with a value of 24.32 ng/ml over 30 day period. Furthermore, it was realized that the high final concentration value is likely because of small size of buffer. Case 2 provides a high value of concentration with an average value of 53.63 ng/ml over 30 days. The average gradient is about 7.5 ng/ml over 30 days (only first half of lumen). The average concentration in lumen for Case 3 over 30 days is 44.71 ng/ml. The average gradient in this case is 45.33 ng/ml. Case 4 provides a very low gradient (2.2 ng/ml) even over just half length of lumen and an average drug concentration of 20.55 ng/ml. Case 5 provides an average drug concentration of 6.93 ng/ml with average gradient of 7.89 ng/ml. Case 6 maintains a low average concentration value but has a very high relative gradient (7.1 ng/ml).

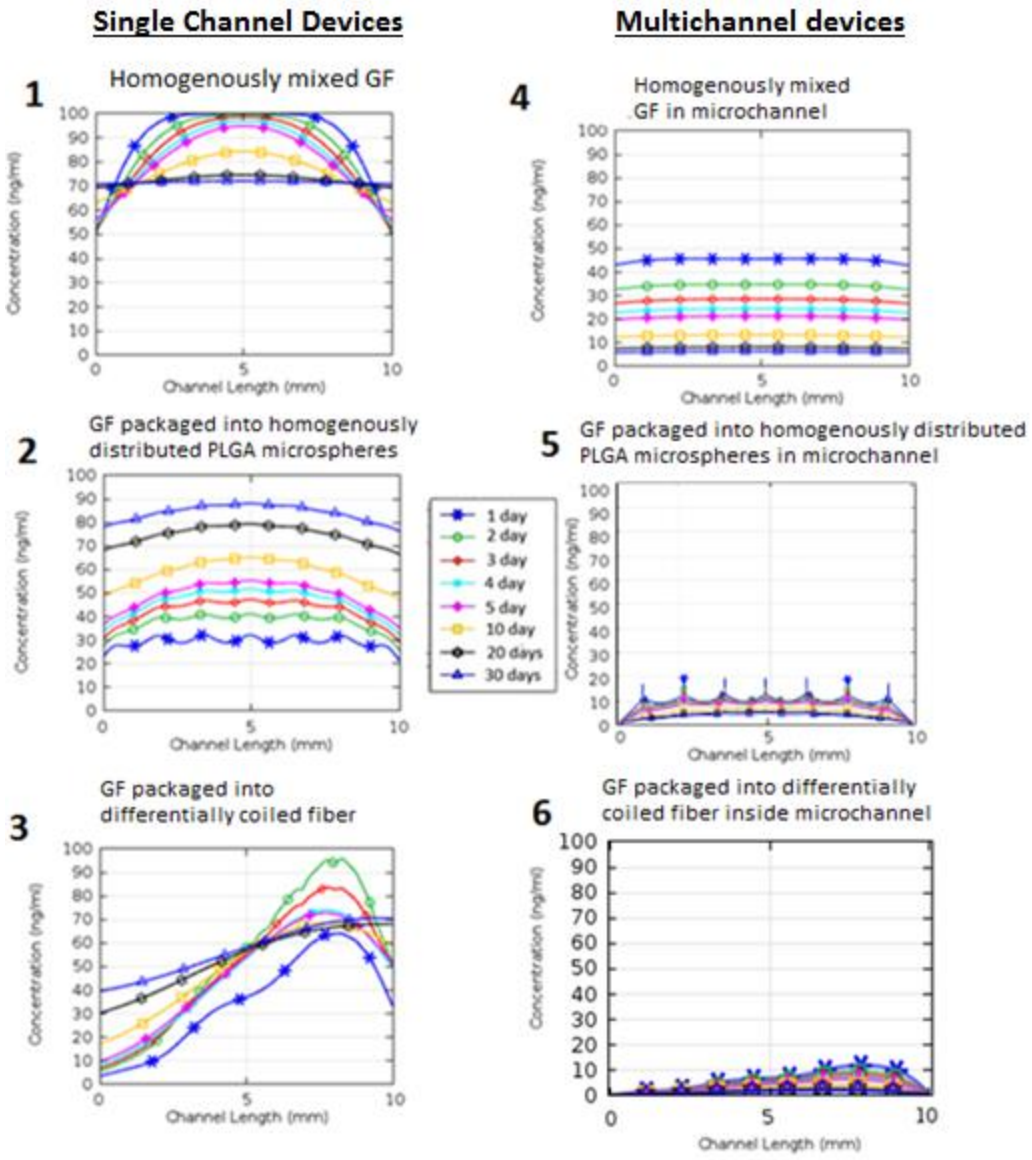

Figure 3-3 Axial concentration variation in the active channel/microchannel for the six designs. The different time points considered are 1, 2, 3, 4, 5, 10, 20, 30 days.

The average concentration values for time points 1, 2, 3, 4, 5, 10, 20, 30 days are summarized in Table 3.1.

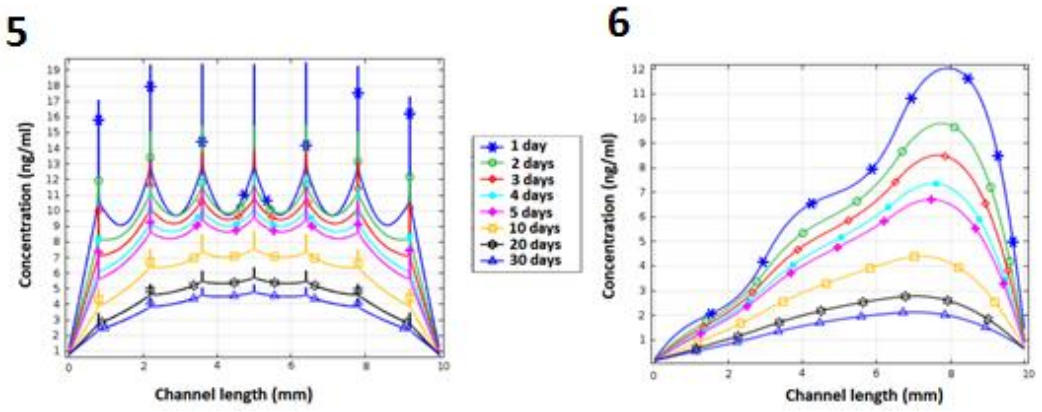

Figure 3-4 Scaled up versions of plots for 5 and 6 in Figure 3-3

A major difference between single channel and multichannel models is that there would be a significant loss through the circumference of the microchannel, and not just the axial ends. This is attributed to the high surface area that the microchannel circumference is exposed.

Table 3-1 Average concentration values (ng/ml) for six different cases at 1, 2, 3, 4, 5, 10, 20, 30 days

C (ng/ml)	Time							
case	1 day	2 day	3 day	4 day	5 day	10 days	20 days	30 days
1	90.49	86.87	84.24	82.24	80.67	75.95	72.54	71.68
2	28.49	33.49	41.02	43.56	52.06	66.12	80.90	83.43
3	32.87	38.14	40.38	42.46	43.29	48.62	53.99	57.96
4	45.25	34.38	28.17	24.05	13.15	8.06	6.26	5.10
5	9.76	9.00	8.34	7.72	7.29	5.61	4.18	3.53
6	4.08	3.42	3.04	2.69	2.55	1.72	1.15	0.91

The surface area for the end of microchannel and circumference can be calculated according to $2\pi r^2$ and $2\pi rL$ where r and L represent radius and length of

microchannel. The values comes out to be 49086 um^2 and 7850000 um^2 for the total end area and circumferential area respectively, The circumferential area is about 160 times that at the ends. Therefore, it is anticipated that radial leak to surrounding agarose would be significant.

3.3 The Coil Configuration

We now focus our attention to coil configuration to observe how differential coiling affects the concentration distribution. The two modeled designs contained 78 coil turns and had only one difference: one design had uniform coiling configuration (U) and other had a differential coiling configuration (G) with 4, 27 and 47 distributed evenly over 10 mm length.

Figure 3-5 shows the difference in concentration variation. The color bar shows the range of concentration variation observed in the lumen (0-13 ng/ml). The U-configuration model allows a bidirectional diffusion of drug through either sides of the lumen as well as equally through the circumferential surface area of microchannel. And the chemotactic gradient is only present for the first 2 mm of the microchannel. Whereas, in the G configuration, since the coil is densely packed near the distal end, concentration is higher in that region which allows for formation of an axial chemotactic gradient. The gradient extends up to maximum of 78% deep into the channel length, something highly favorable for axon growth since it is desired axons try to reach up to the distal nerve stump.

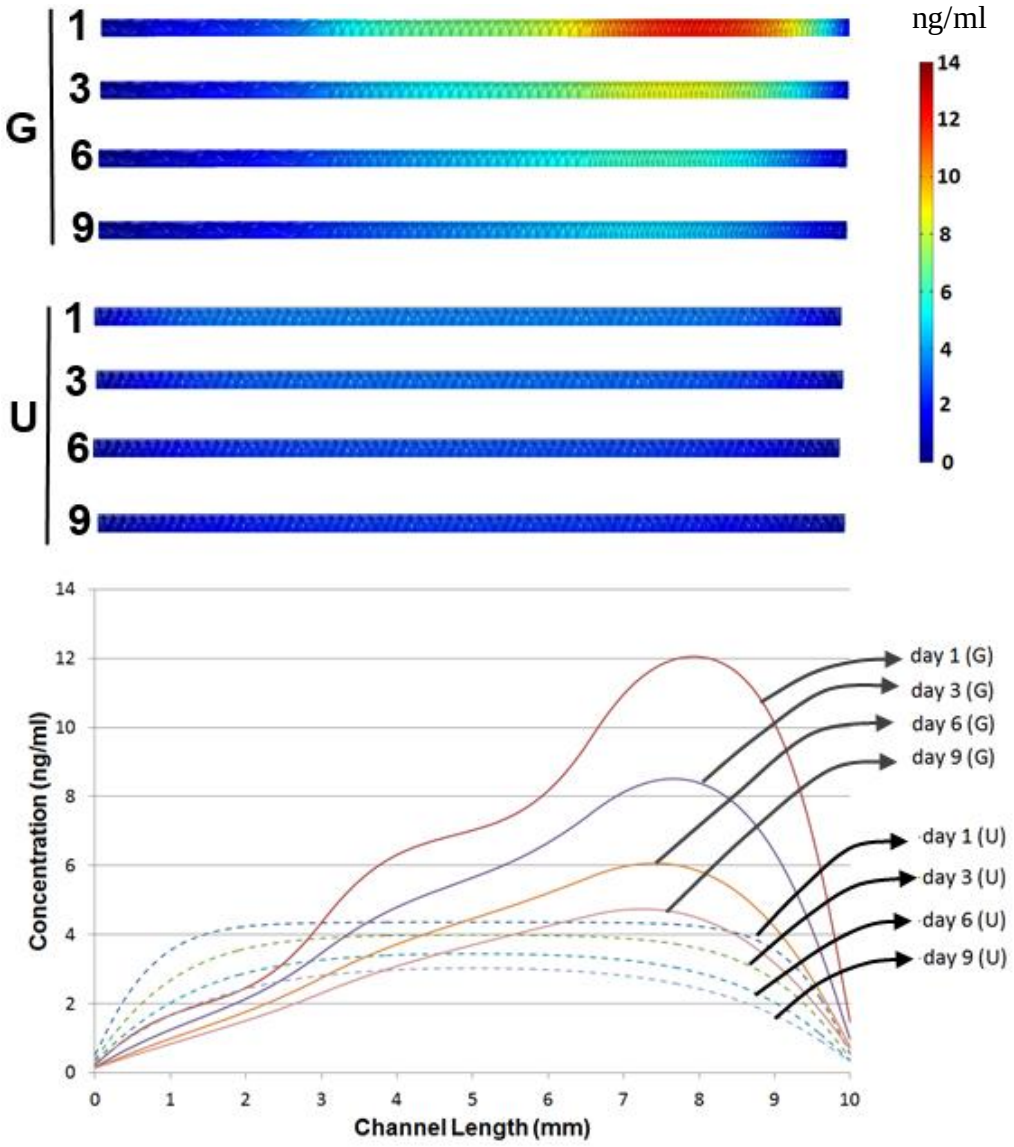

Figure 3-5 Computer simulation data for uniform (U) and gradient (G) coil models obtained from COMSOL Multiphysics for 1, 3, 6 and 9 days. The difference in concentration between U and G configuration can be observed in the microchannel. Concentration vs channel length plot showing positive gradient exists upto 78% channel length for G model.

The axial concentration gradient varies from 1.33 ng ml^{-1} mm^{-1} at day 1 to 0.8 ng ml^{-1} mm^{-1} at day 9 for G model. The value is higher for U model at around 2 ng ml^{-1} mm^{-1} but only extends up to first 2 mm against 7.8 mm in G model.

3.3.1. Axon Straightness Evaluation

While the G model is able to create a one sided gradient as compared to U model, we also want to see how much would growing axons diverge from a linear path. For this, we utilize the Radial diversion technique discussed in section 2.5. Using Particle tracing in COMSOL post-processing we released a particle from (42 um, 42 um, 0), i.e. from the starting plane of proximal nerve stump. The particle was release from day 1 to day 5 with time-step of 1 day. This was done in the exactly same manner for both U and G models. The resulting particle trajectories through the microchannel are shown in Figure 3-6.

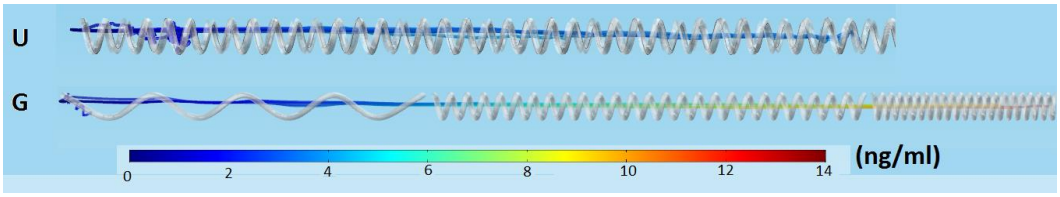

Figure 3-6 Visualization after doing particle tracing for both U and G models respectively. The particle starts from (42 um, 42 um, 0) and was released till 5 days with every step being 1 day. The color field represents the concentration magnitude (ng/ml). The par

The trajectories were assigned a thickness of 8 microns for easy visualization. These trajectories were then color coded according to local concentration magnitude. The co-ordinate data was then extracted from the software and analyzed in Microsoft

Excel. From the visualizations it can be seen the trajectories only extend up to 50% of the channel length for uniform configuration against around 78% for gradient configuration.

We only consider trajectory co-ordinates for first 5mm of both designs for fair comparison. Radial diversion was calculated for both models as explained in section 2.4. RD for U and G models was calculated to be 52.3 um and 30.3 um respectively.

3.4 Effect Of Coil's Major Radius

For the current NGC designs discussed above that have the differential coil configuration; the coils almost stick to the walls of the lumen (Figure 3-7).

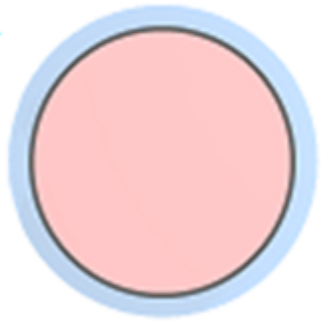

Figure 3-7 Cross-section view of a single channel gradient configuration device The grey ring represents coil and pink represent collagen respectively.

Because of this geometry, the drug delivery direction gets concentrated towards the center point, which can lead to a relatively large localized radial gradient. And this local radial gradient can cause the axons to diverge. We compare two designs and observe how the radial gradient problem can be minimized. Figure 3-8 shows two different designs: first one has coils sticking against the wall of lumen and second one has a smaller major radius.

In design A in Figure 3-8, all the drug molecules get released radially inwards, while the same amount of molecules get distributed radially inwards and outwards in design B. This way the gradient is broken into two individual smaller gradients. Computer simulation was done to observe this phenomenon up to 4 days with time stepping of 4 hours. For design B the major radius of coil was reduced by 30%. Everything else was kept same.

Figure 3-9 and Figure 3-10 show cross-sectional plots along a diameter through 3 different cross-sections for design A and design B. The cross-sections are located at 1, 5 and 8 mm from the axis start which is the end of proximal buffer. Oscillation is observed in which gradient changes from negative to positive in the three cross-sections for both configuration. As expected, there are two gradients in the latter design. An interesting observation can be seen from the plots: it takes just 1 day for the modified design for the concentration to become radially uniform as against 4 days in the first design.

Because of the nature of radial fluctuations, different axons starting at different radial positions at the proximal nerve stump will see different positive/negative gradients in either of the designs.

For example, in the first design, an axon that starts from center of axis from the proximal stump before 24 hours will start growing towards the coil because of higher concentration available near the coil. But if the same axon starts growing after 24 hours, it will keep on traveling straight axially since maximum concentration is available in that direction.

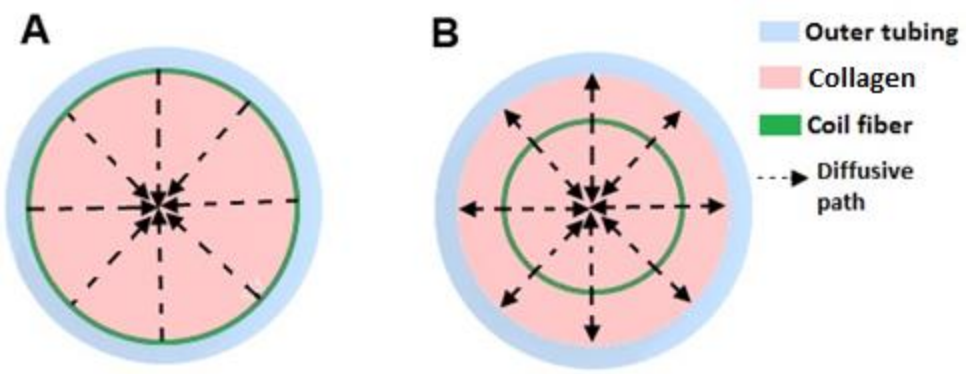

Figure 3-8 Difference in drug delivery direction in two different configurations: A) Drug molecules only travel radially inward, but in B) travel radially inwards as well as outwards. Therefore in B, the gradient is broken into two smaller gradients.

On the other hand if an axon starts growing before 24 hours from the maximum radial position on the proximal stump, it will either keep traveling straight or attach to the coil. But if it starts growing from the same point after 24 hours, it will travel towards the center of channel since maximum concentration is available there.

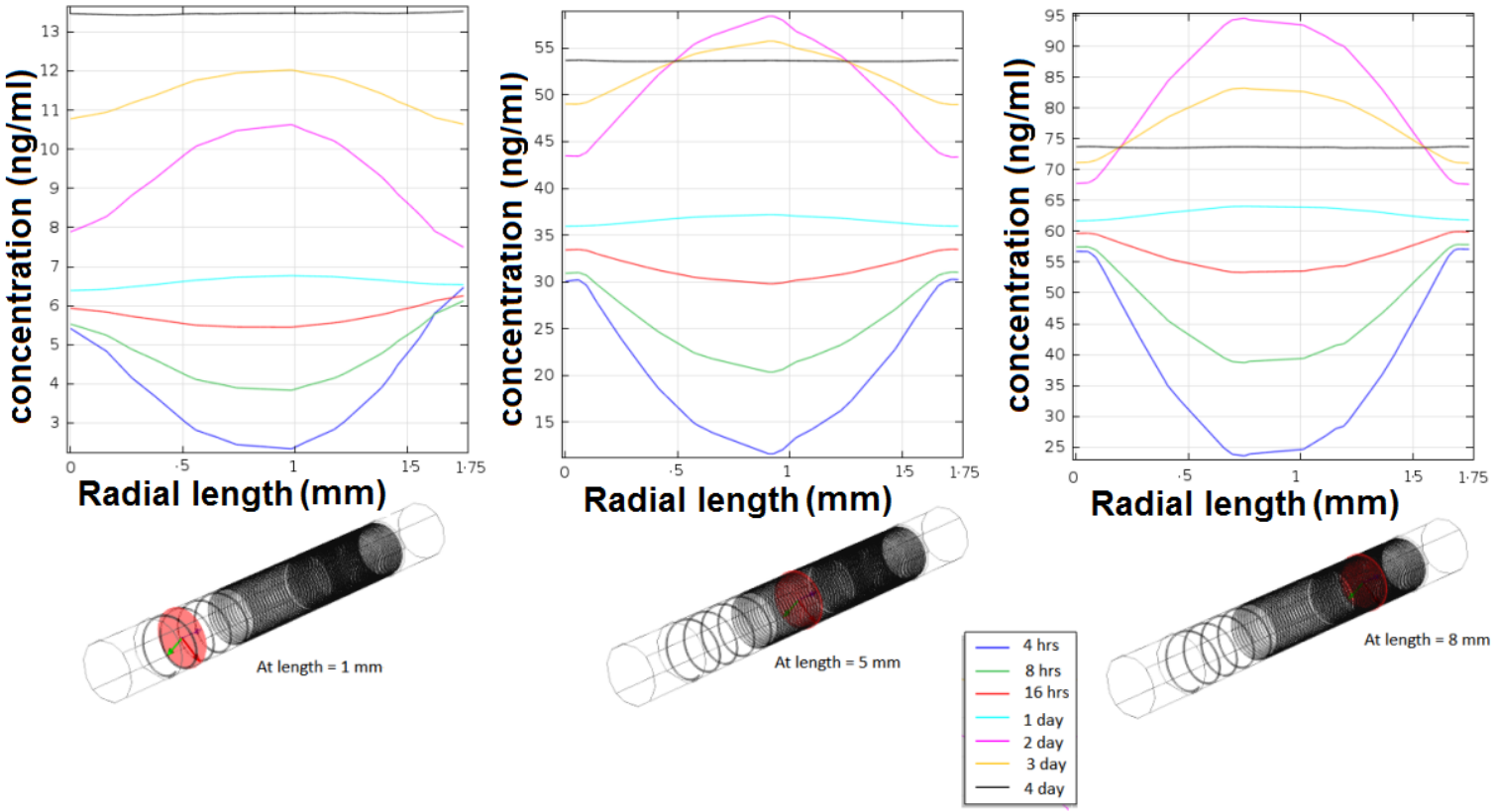

Figure 3-9 Cross-section concentration plots for design A. The cross-sections are located at 1, 5 and 8 mm.

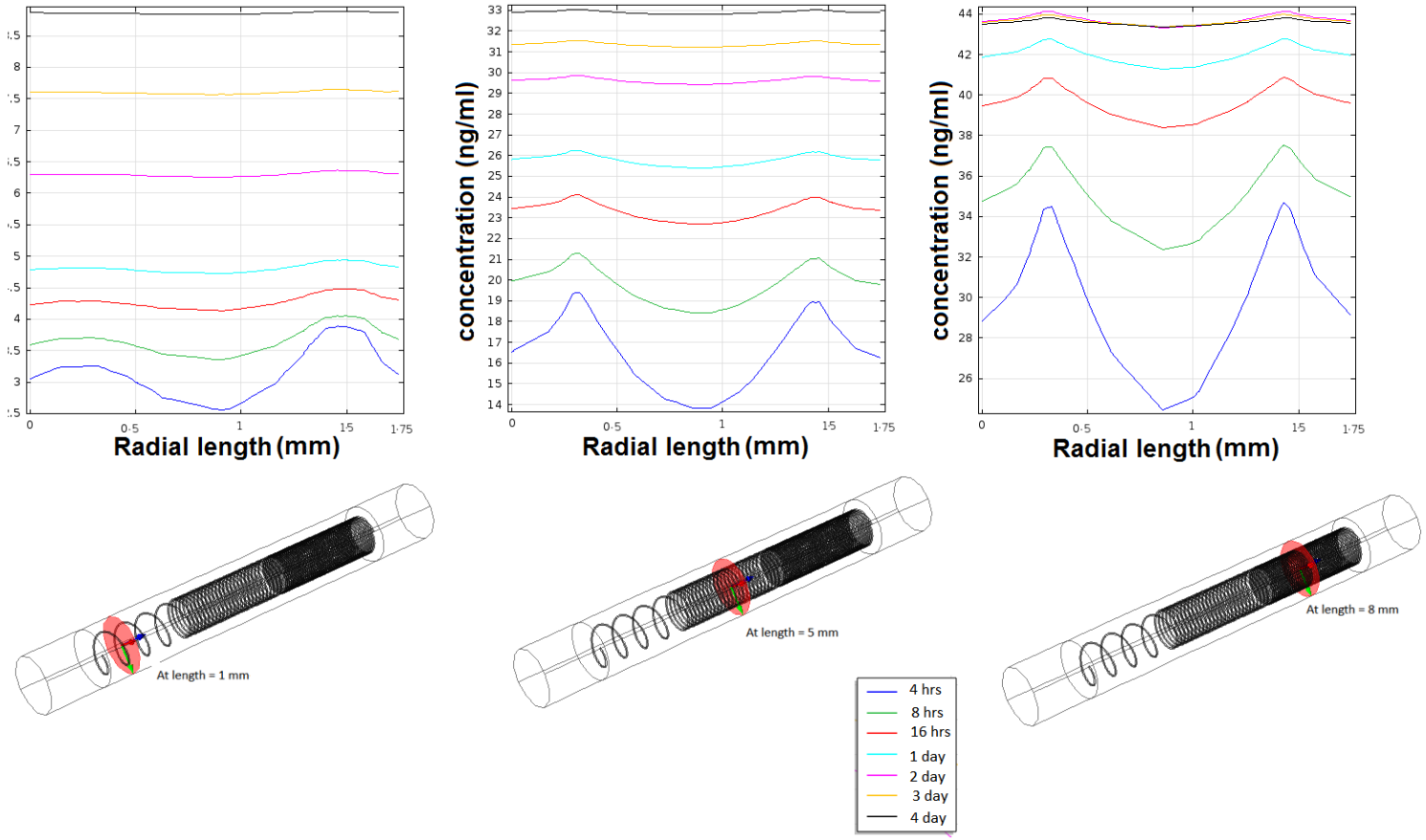

Figure 3-10 Cross-sectional plots for concentration vs length (radius) for design B. The three cross-sections are 1, 5 and 8mm from axis start (buffer-device interface).

3.5 Effect of microchannel size

It has been experimentally shown that using multiple channels[10] of small radius are able to guide the axons much more efficiently to their distal target. Based on our understanding of radial dispersion, it seems that the most probable cause of superior performance of small size channels that radial axonal divergence is minimum. To confirm this, 4 different multichannel models were made using coil configuration. The channel radius for each model was 125, 187, 250, 310 micrometers. As done earlier, the models were compared to a baseline 100ng/ml value, and the release from coil for adjusted accordingly.

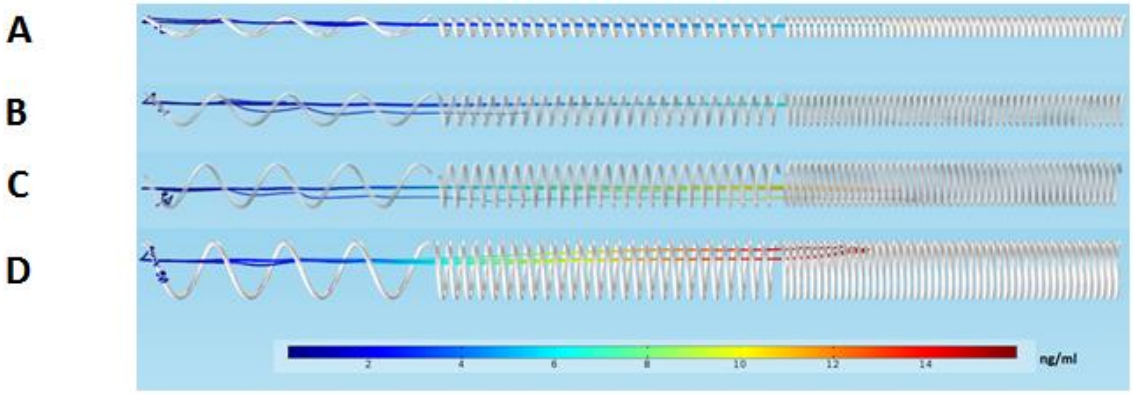

Figure 3-11 Computer results of trajectories of a particle released from one third the distance of channel radius. A, B, C and D have 125, 250, 187, 310 um radius respectively.

Particle was traced in each of the 4 models starting from the start of microchannel. The radial co-ordinates were fixed at one-third of channel radius in each case. The visualization of particle tracing is summarized in Figure 3-11.

A common observation in all 4 models is that the particle is attracted towards the first turn of coil near the proximal end. Another common feature is that the depth to which positive gradient exists is approximately same in all 4 cases (74-79%). The variation of radial dispersion vs the channel radius is shown in Figure 3-12. The variation is almost linear with correlation coefficient of 0.986. The RD parameter according to the linear equation is 0.685r+54.29 where 'r' is the radius of microchannel.

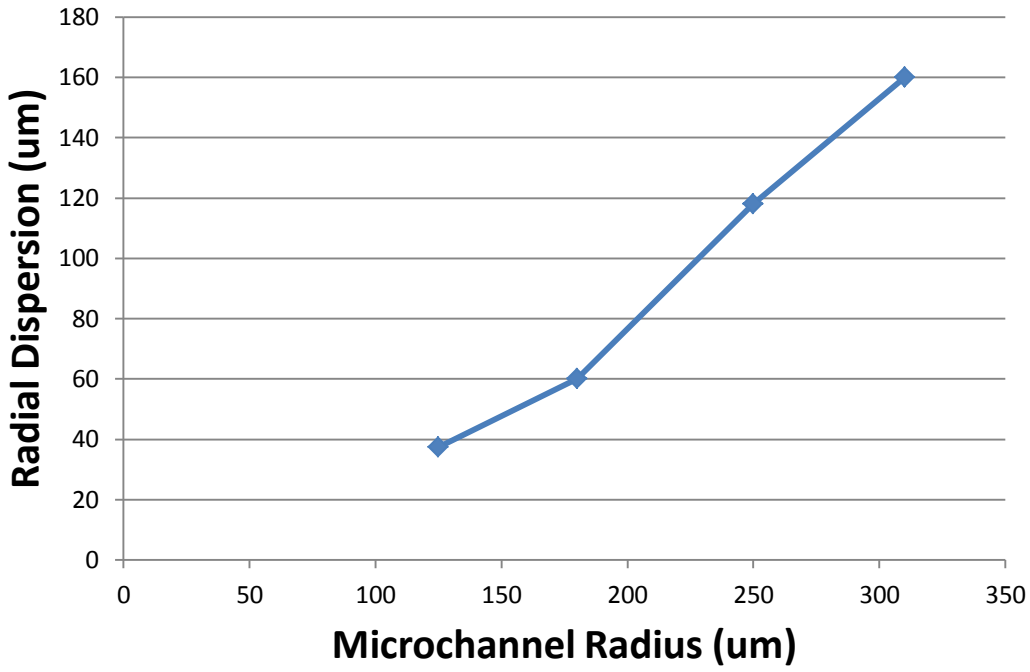

Figure 3-12 Plot of radial dispersion (RD) parameter vs the microchannel radius,. The variation is almost linear with correlation coefficient of 0.986.

Chapter 4

Discussion

From our results, it is evident that temporal maps of drug distributions in the NGC can be very different depending on the method of delivery or by changing the geometry of the same design. Figure 4-1 summarizes the average concentration value as well the average positive gradient in different designs (averaged over 30 days).

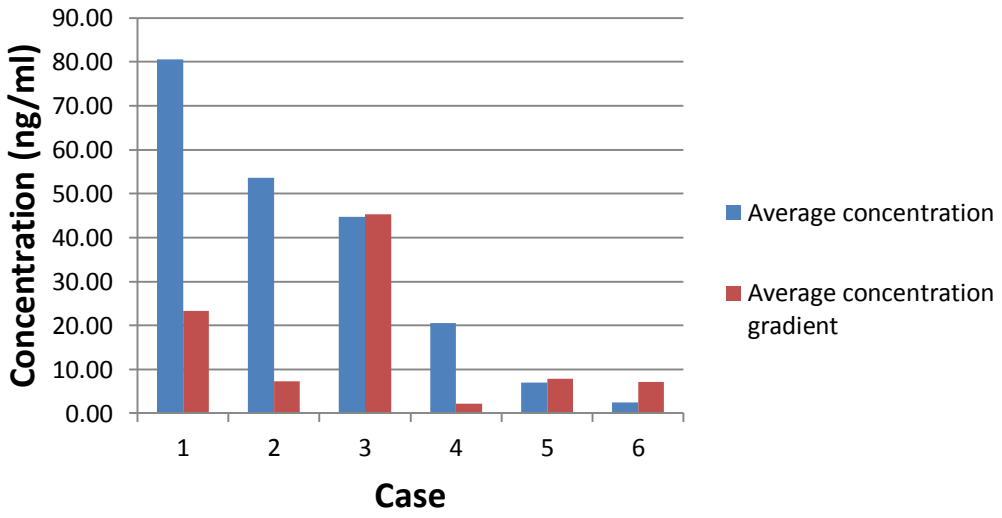

Figure 4-1 Average concentration and peak concentration gradient averaged over 30 days for the six designs.

It can be seen from Figure 4-1 that the magnitude of average concentration and average concentration gradient are strongly affected by the method of drug delivery and the channel sizes. It is clear that designs 3, 5 and 6 are able to maintain a strong concentration gradient relative to their respective average concentration value. This can have strong implications experimentally since it's the positive concentration gradient that

guides the axonal growth linearly and not the concentration value itself. A simple thought experiment elucidates this fact (Figure 4-2). Following this, we calculated the ratio of average concentration gradient and concentration over 30 days. The results are shown in Table 4-1. It can be seen that Case 6 has the highest (Δc/c) value as well as a high concentration gradient depth. This could be a possible explanation for why multichannel devices perform better[10]

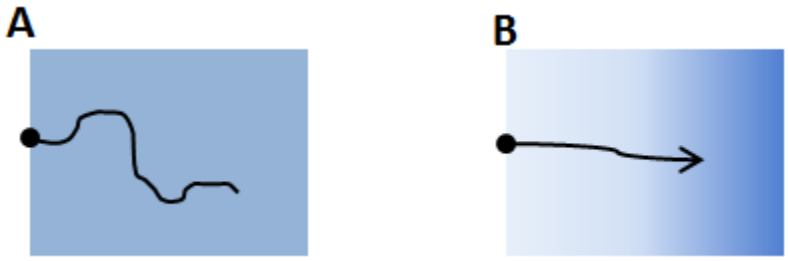

Figure 4-2 Thought experiment to understand the effect of concentration and concentration gradient. The black dot represents start of axon and black line represents axon. (A) contains uniform concentration field at value c and (B) contains an axial concentration gradient.

We also calculated the percentage of initial drug loading that exists in the channel. This is also the drug that is available for consumption by axons at given point. The drug available in the channel can simply be calculated using equation 18.

$$\text{Amount of drug} = \iint_0^L C \, dz \, dA \tag{18}$$

where c is the local concentration at an infinitesimal small volume of thickness dz and cross-sectional area dA. Although, here we have multiplied the average calculated concentration in a channel with the volume of channel (A*L). The variation of percent available drug for 30 days is shown in Figure 4-3.

Table 4-1 (Δc/c) ratio and gradient depth for different cases.

Case	$\frac{\Delta C}{C}$	Gradient depth (approx)
1	0.29	50%
2	0.135	50%
3	1.01	78%
4	0.107	50%
5	1.138	50%
6	2.91	78%

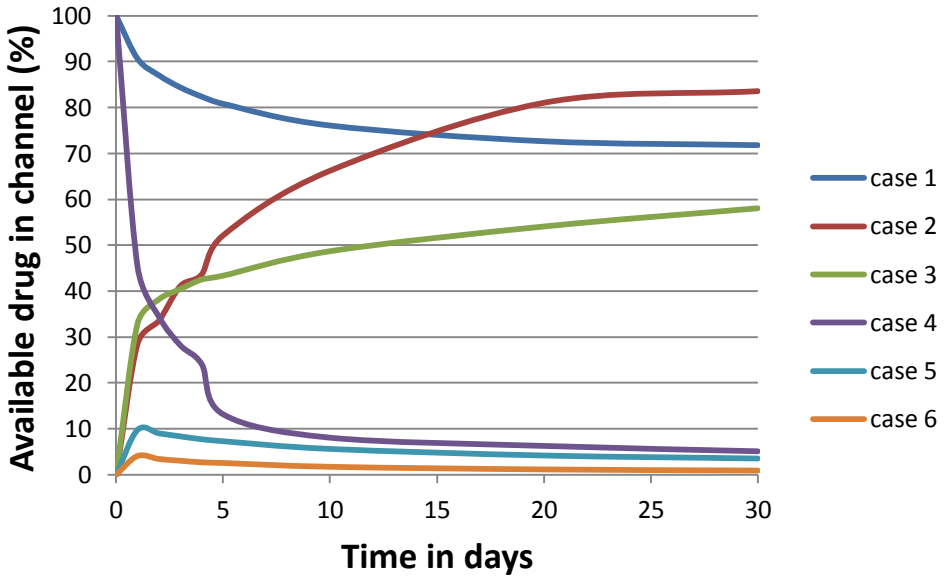

Figure 4-3 Variation of available drug in modeled channel for six different cases.

It can be seen from Figure 4-3 that the available amount of drug increases with respect to time for Case 2 and 3 whereas it decreases for Case 1, 4, 5 and 6. For Case 4, 5 and 6, the low value can possibly be attributed to the leakage that occurs to the surrounding agarose from the channel. While in Case 4 where the microchannel is at 100 ng/ml concentration initially, the loss is rapid with around 85% of drug lost within 5 days. On the other hand, for Case 5 and 6 the loss is most likely continuous because of controlled release. The only leakage that occurs in Case 1, 2 and 3 is via the ends of channel. It is also seen that for Case 1, 2 and 3 the final value stays relatively high even at 30 days. This could mean that the buffers are getting saturated and that their size needs to be increased.

In context of advantage of differential coiling models, designs with non-coiling configuration produce a central high point for drug configuration, whereas differential coiling produces high concentration near dense coiling. Therefore, when the axons growing from proximal end would reach the central region in Case 1, 2, 4 and 5, they would encounter a negative concentration gradient for remaining 50% of length leading to slowing in growth. On the other hand, since concentration gradient extends up to ~78% of channel length in differential coiling configuration, axons would only encounter 22% of remaining length as negative gradient. This is evident from experiments which showed the average axonal length in G configuration to be 60% more than U model. The effect of uniform vs differential coiling is also very clear from axon straightness study. The RD parameter for the uniform model is 52.3 um while the value reduces to 30.3 um for differential coiling model. There is a 42% reduction in axonal radial dispersion. Previously, lab experiments were done to investigate the effect differential coiling. Briefly, a custom device with two wells was used (Figure 4-4(A)). A metal rod with coiling on it is introduced inside the main well of device. Agarose is poured over this well and once

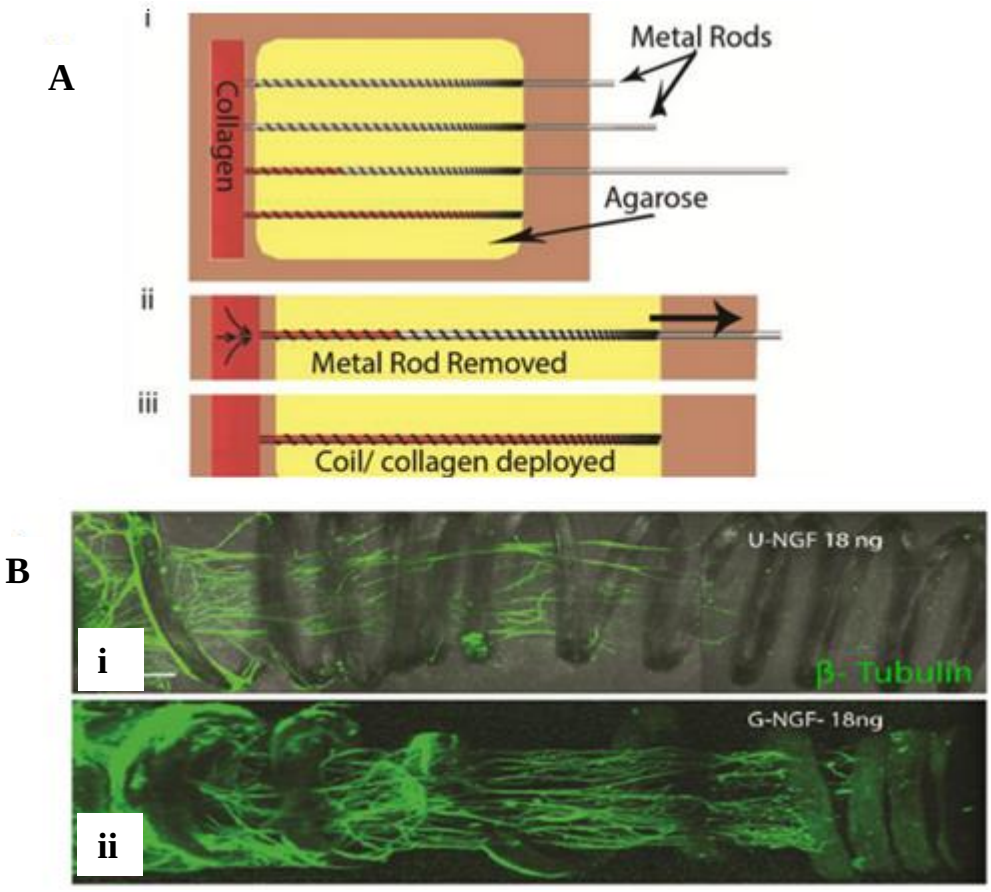

Figure 4-4 (A) Setup for creating collagen filled microchannel. Removal of metal rod creates negative pressure for the collagen to fill the microchannel volume (B) Confocal images of DRG response to i) uniform coiling and ii) differential coiling. Axons can be seen growing more linearly in B (ii). [Image from Nesreen et al]

it solidifies the rod is slowly removed creating a suction effect and pulling collagen from other well inside the microchannel. This way the rod gets removed while the coil remains in place. On observing the confocal images of slices in the microchannel at the end of 7 days, axons can be seen growing more straight in G model as compared to U model.

Using the confocal images, axonal diversion was showed to be reduced by 50% in U model as compared to G model[36]. The effect can be seen in Figure 4-4(B). The phenomenon of axons coiling around the first turn is also seen in almost all computer particle tracing results. This happens because at earlier times (<4 days), the radial gradient dominates and the net concentration vector directly guides the axons towards the first coil turn.

The straightness of axon does not only depend on the coil configuration, but also on the channel radius. In Figure 3-12 it is clear that radial dispersion increases linearly as radius of channel increases. The variation follows the linear equation 0.685r+54.29 where 'r' is the radius of microchannel. This has important implications since approximate estimates for specifications for radius of microchannel can be known before hand for experiments.

In section 3.4, we also analyzed the effect that coil's major radius has on the radial concentration distribution. The motivation for doing this was to break down the high radial gradient to two smaller radial gradients. And the results demonstrate in the first zone with 4 coil turns, the radial concentration oscillates between positive and negative and settles by 4 days. Whereas in the modified design B, the concentration is almost uniform by end of first day. This suggests any axons that are sprouting from the proximal nerve, will grow relatively straight in the modified design as compared to the initial design A. This oscillation of concentration gradient is also seen in the second and third zones of coiling. In both the zones, the value settles to almost uniform by end of day 1 for modified design B as compared to 4 days for initial design A. Although the main region of concern is the first zone since axon would most likely take more than 4 days to reach the second and third zones. It is also possible that the modified design B will see less or no axons

coiling around the first turn since radial concentration gradient is less and becomes uniform within a day.

Incorporating PLGA microspheres is a good way to achieve control release, but they fail to create a chemotactic gradient. It is also likely that the microspheres themselves hinder the growth of axons. There can be two reasons for this. One would simply be the size of microspheres which is relatively large (5 um diameter). Another cause for this can be since axons sense the local chemotactic gradient present at micrometer scale, microspheres present around an axon growth cone create local disturbances in the concentration and essentially “confuse” the axon. This can be understood from Case 2 in Figure 3-3. There are multiple local gradients formed within the channel. There are only 63 and 35 microspheres that are modeled with computer model, but in reality there might be hundreds of microspheres present. Therefore hundreds of local disturbances at micrometer scale can be expected. The illustration of this phenomenon is shown in Figure 4-5. The axon can deviate from its desired path if it senses a stronger chemotactic gradient in its surrounding from a nearby microsphere.

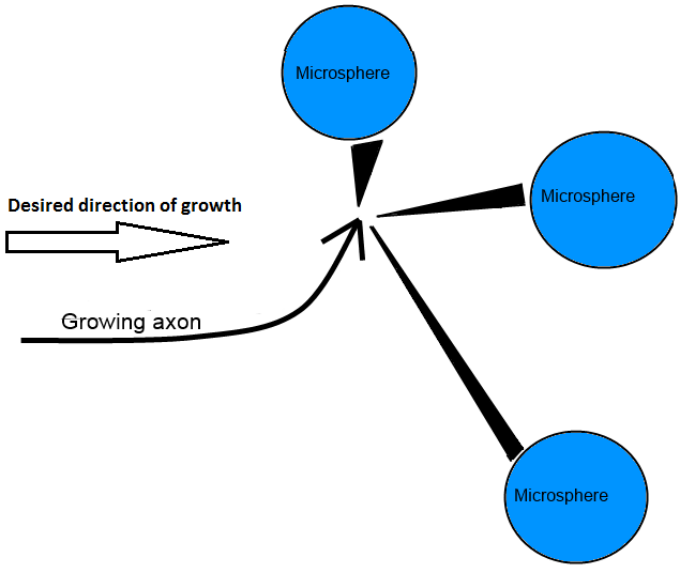

Figure 4-5 A growing axon senses chemotactic gradients at micrometer scale and can be deviated from the desired path because of stronger local gradients from nearby microspheres.

4.1 Limitations

The computer models do not account for temperature and pH changes since we want to keep the parameters to the minimum to keep the model simple for it to be solved. Although a model for drug consumption by the axons in the NGC microenvironment has been developed, it is not implemented in the computer models. Therefore it is anticipated that the concentration values obtained would be higher than real values. The magnitude of this difference is not known. Although, particle tracing coupled with radial dispersion parameter have been used as a technique to quantify axon straightness, it should be realized that experimentally, the values might be different. This is because the quantification method here only takes into account the chemotactic gradient and ignores any effects of structural and mechanical properties of substrate. Furthermore, particle tracing protocol does not take into account the magnitude of positive chemotactic

gradient. Any value for gradient above 0 is considered for tracing. In reality, there might be a threshold minimum value of positive chemotactic gradient which the axon growth cone can sense and follow. This is evident in Figure 3-6 in section 3.3. The gradient is negligible for U configuration model after 2mm but the particle still goes up to 50% channel length since it senses >0 concentration gradient value.

Chapter 5

Future Work

5.1 Newer computer models

The models developed were used to simulate the spatiotemporal concentration variations in drug diffusion and to predict the trajectories for axonal growth. The axon trajectories are probable paths that a growing axon might take. The approach of particle tracing does not assume any mass for the particle and they do not experience any drag force. Future computer models could assign more realistic physical properties to these particles, so that the trajectories could correlate better with experimental observations taking these additional effects into considerations.

Section 2.6 discusses in detail about receptor-ligand kinetics. Such mathematical models can be coupled with the existing physics of computer models to get even more accurate results. Understanding receptor-ligand kinetics allows for formulation of how fast the drug gets consumed by axons. This rate of consumption can be specified in the model. And based on the amount consumed, axon growth model can calculate the growth trajectory of particle. Based on the model developed in section 2.6 a preliminary design was made in COMSOL which would account for the rate of consumption. The cylindrical disk was assumed to be stationary and of thickness 1 mm as shown in Figure 5-1. Although the model was meshed successfully, it did not solve.

Along with rate of consumption, future models can also account for axonal growth. The proximal cylindrical disk modeled in Figure 5-1 can be assigned physics based on an axon growth model (see appendix E). Newer models can also incorporate the degradation rate of the main filler hydrogel. Mathematical modeling degradation is challenging in our context since there is no uniformity in it, i.e., degradation would

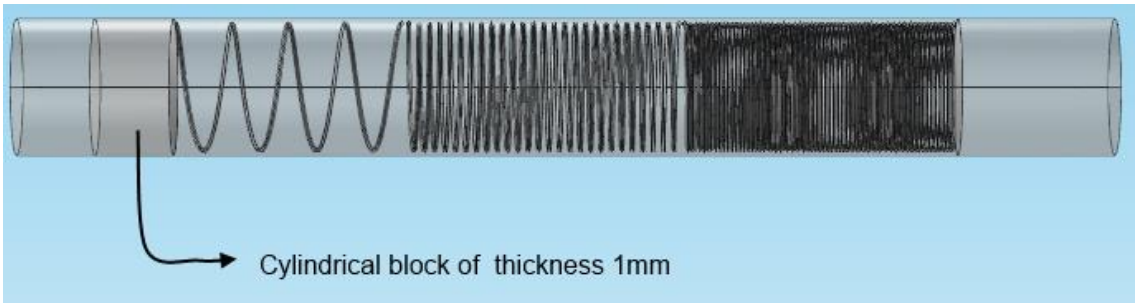

Figure 5-1 COMSOL geometry of model developed to account of rate of ligand consumption.

not be strong enough from the sides of device since it is protected by the tubing. Although, significant amount of degradation would be present at the active region where axonal growth is happening. There would also be considerable degradation at distal end since the end is exposed to living tissue. Mathematical models usually account for surface or bulk erosion when the entire surface is exposed. Although if experimental data is available regarding spatial degradation rates for the specific device, the data could be incorporated in the design. This data would have to be applied very carefully since one end in the device grows while the other stays stationary.

A key aspect of differential coiling design is the positive gradient depth to which it extends inside lumen. Current design allows for positive gradient to extend up to 78% of channel length. This can possibly be increased by making changes to coil geometry, specifically the pitch of coil. Current design uses three discrete segments of coils, and the pitch does not vary in a continuous manner. If the pitch is assigned in a form of equation, gradient penetration can possibly be increased. A model was designed and meshed to observe this phenomenon (Figure 5-2). A parametric curve was used to model the variable coil pitch. Unfortunately, meshing helical geometries is a challenging task and the model did not solve despite multiple meshing efforts

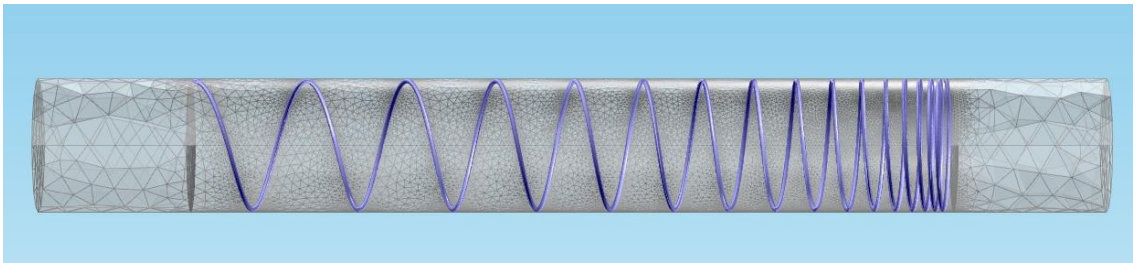

Figure 5-2 A design that was modeled to increase the positive gradient penetration.

New computer models could also take advantage of 3D reconstructed data from experimental results. For example, if axons are reconstructed for time points of 1, 3, 6 and 9 days, RD parameter could be calculated from their co-ordinates and correlated with the values from particle tracing. Furthermore, average growth rate of axons could also be calculated from the experimental data. An attempt of 3d reconstruction of data obtained at 7 days is shown in Figure 5-3. Note how data is very unclear from front view. This

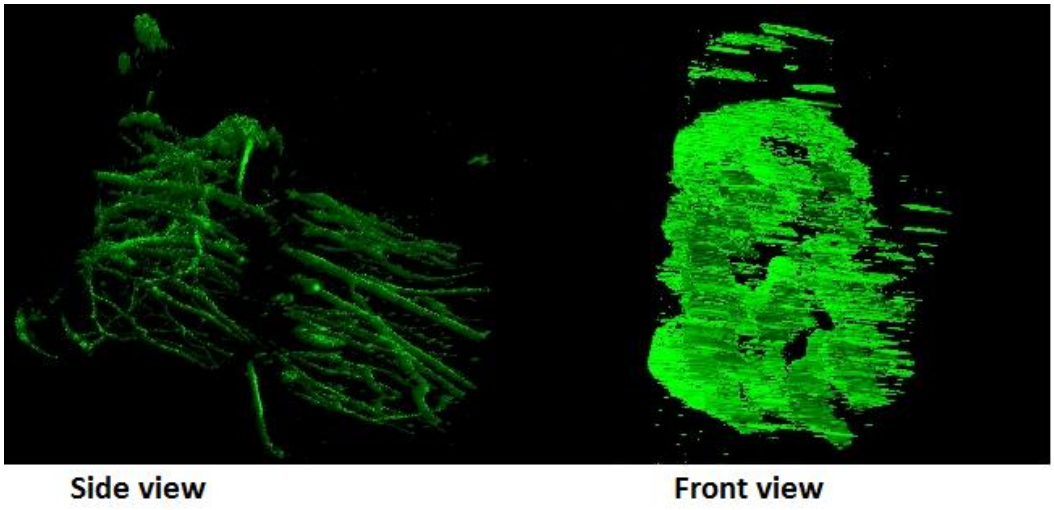

Figure 5-3 Side view and front view of 3d confocal data obtained at 7 days.

happens because the slice distance in the confocal data for this particular data set was 15.4 um, which is very high. Most axons growing inside the lumen are about 3-6 um thick. Therefore an ideal slice distance for accurate reconstruction would be about 2-3 um.

Simulations such as ones discussed in this project can be used to evaluate the performance of other newer designs. For example, if multiple growth factors have to be used in a single device, the concentration profiles of individual species can be tracked accurately. Nutrient holes that are made on the circumference of the main device for providing nutrient support for the growing axons can also be modeled. If we know the specific nutrients, their diffusion into the device can also be tracked. Furthermore, if mathematical algorithms such as that of axon growth model are coupled with the diffusion model, we can get even more accurate picture of how the axons might behave.

Chapter 6

Conclusion

The results shown above in this project show how computer modeling can be used to understand the physical phenomena before experiments are conducted. The concentration profiles in different designs can be compared with each other to evaluate which one would be most optimal. It is difficult to measure the spatiotemporal concentration variations inside a device experimentally. There are only a limited number of data points that can be obtained experimentally. The work done in this project elucidates the methods and protocols through which axonal growth inside NGC can be quantified. Specifically, the protocol to quantify axonal straightness can be applied in many different models. We could further apply the method to predict how linearly axons grow as can be seen from experimental results. Overall, this work shows:

1) different drug delivery mechanisms produce different spatiotemporal concentration as well as concentration gradients.
2) axon straightness protocol can can be used to estimate axon linearity in different designs.
3) axon linearity increases if coiling in microchannel is differential.
4) radial concentration disturbances reduce if major radius of coil is reduced.
5) axon linearity increases as size of microchannel decreases.
6) drug consumption rate, average growth rate and local concentration gradient can be coupled together with the diffusion models so that particle tracing would yield even more realistic results.

Appendix A

Diffusivity Calculation

Diffusion is a mass transport phenomenon which happens without any bulk movement. Diffusivity is one of the most important parameters when doing a diffusion study. For a molecule in a liquid, the diffusion coefficient can be obtained according to Stokes-Einstein equation[18]:

$$\mathrm{D}_0 = \frac{k_B T}{6\pi\mu R_h} \qquad \text{Eq. (A1)}$$

The equation takes into account the hydrodynamic radius of the solute molecule assuming it has spherical shape. k_B is Boltzmann's constant = $1.38\text{x}10^{23}$ J/deg. The equation also relates to solution viscosity μ and temperature T (Kelvin). R_h, the hydrodynamic radius of the molecule can be calculated as[18] equation A2.

$$\mathrm{R_h} = \left(\frac{3\mathrm{MW}}{4\pi\rho\mathrm{N_A}}\right)^{\frac{1}{3}} \qquad \text{Eq. (A2)}$$

where MW is the molecular weight (kg/mol) of the solute (NGF here). ρ is the density of the solute molecule sphere and N_A is avogadro's number (mol^{-1}).

Diffusivities can be measured by different methods. One such method is to use the effective medium model along with carman-kozeny model to estimate permeability[11]. Diffusion coefficient D in the substrate is can also be calculated according to Renkin equation[18].

$$\frac{D}{D_0} = \left(1 - \frac{a}{R_h}\right)^2 \left[1 - 2.1\left(\frac{a}{R_h}\right) + 2.09\left(\frac{a}{R_h}\right)^3 - 0.95\left(\frac{a}{R_h}\right)^5\right] \qquad \text{Eq. (A3)}$$

Appendix B

Meshing Example

Consider an example of a wheel rim[39] under static load. , The major forces act on the radial arms (spokes) connecting the center region to the outside circumference of rim (Figure B-1)

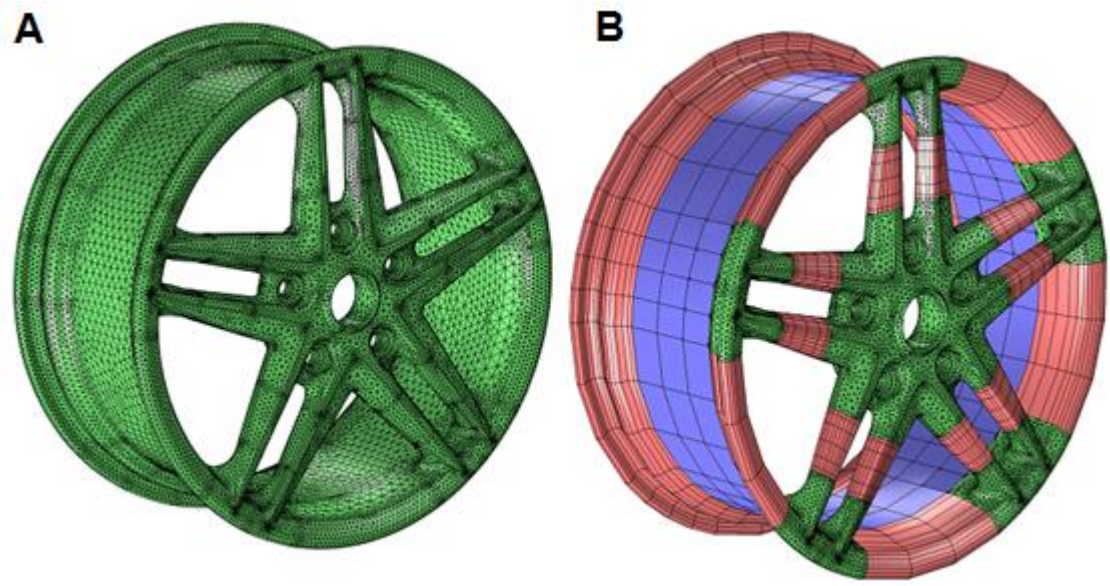

Figure B-1 Different meshing strategies can be used for same geometry depending on the critical load bearing regions. A contains only tetrahedral elements while B contains a mixture of different element types[39]

The rim on the left in Figure B-1 used tetrahedral elements completely while the rim on the right used a mixture of tetrahedral (green), bricks (blue), prism (pink) and pyramidal elements for transition. It can be seen that small tetrahedral elements are used in the critical regions where load transfer takes place, while the circumference is meshed with large brick elements since no major load transfer takes place there.

The meshed geometry on has about 145000 tetrahedral elements while that on the right has 78000 mixed elements. Both geometries will solve correctly for same loading case, except the one the right takes about half the time. It should be noted that to mix mesh a geometry, significant user interaction is needed to for correct and accurate mesh.

Appendix C

Methods to Quantify Axon Straightness

C.1 Sinuosity

First method is my calculating a term called “Sinuosity”, S. This term is mathematically equal to the ratio of shortest trajectory length to actual length of trajectory (equation C1).

$$S = \frac{\text{actual path length}}{\text{shortest path length}} \qquad \text{Eq. (C1)}$$

In Figure C-1, actual path length is represented by the black line, while the shortest path by the red line. Sinuosity S can vary between 1(straight line) to infinity for a closed loop[19].

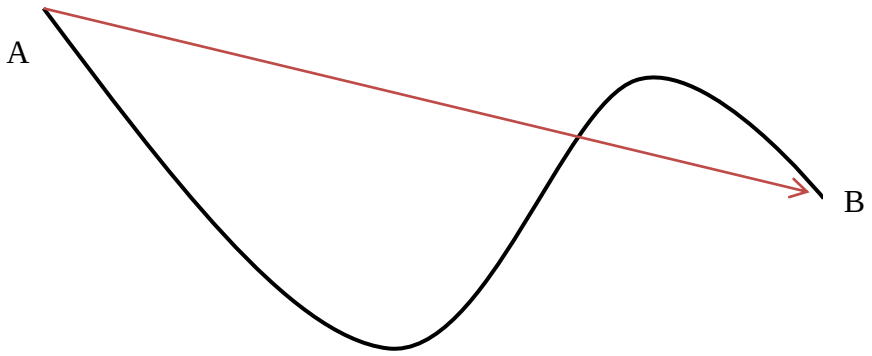

Figure C-1 Schematic of actual and shortest path for calculating Sinuosity.

While this method is seems correct for quantifying axon straightness of an axon, it is decided not to proceed using this method. There is no bounded range between which ‘S’ will come out to be. It is preferred that a parameter that would help us quantify straightness should also physically mean something. This will be evident in the third method.

C.2 Fractal Dimension

Second method that was looked into for straightness quantification was “fractal dimension”. Fractal dimension is a genius concept to measure complexity and is based on work by Benoit Mandelbrot’s 1967 paper on self-similarity[22]. Fractal dimension is occasionally used to

characterize the windiness of rivers and coastlines. For the purposes of straightness of axon, a variant of this method is used here and is given by[21]:

$$D = \frac{\log(\frac{L}{a})}{\log(\frac{d}{a})} \qquad \text{Eq. (C2)}$$

where D is the fractal dimension. L is the total length of axon has travelled, d is the estimate of largest distance actually covered, and a is the average length of a step. Because of the nature of the equation, D will always vary between 1 and 2; 1 being completely straight and 2 being completely random and almost representing a surface. It should be noted that the above mentioned variant of Fractal Dimension is valid for a 2D plane.

When talking about 3 dimensions, such as our case, D varies between 2 and 3; 2 being almost plane (surface) and 3 being completely chaotic and filling up a volume[23]. This method while being a great concept was not used for now. Calculating 'D' in 3D for an axon would require expertise in algorithm writing.

Appendix D

Mathematical Equations Describing Variation in Number of Receptors, Ligands and Receptor-Ligand Complexes

The following brief mathematical analysis[29] formulates the rates of change of receptor, ligand and complexes per unit time.

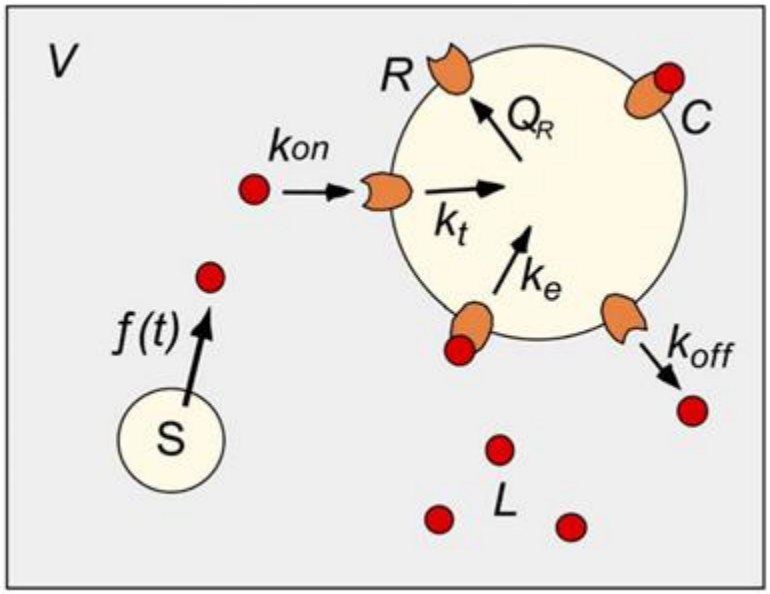

Figure D-1 Different variables involved in receptor-ligand chemical kinetics. S represent a ligand (L) supplying source. V is the active volume in which ligand consuming cells are present.

Assuming S is a source which supplies the ligand L in the volume V at a constant rate f(t). R represents the free receptors on the cell surface (Axon growth cone) and C is the receptor-ligand complex. The ligand is able to reversibly bind to the receptor R with a forward rate k_{on} and reverse rate k_{off} to yield the complexes. The rate of synthesis of free receptor is Q_r. K_t and k_{er} represent rate of internalization for free receptors and receptor-ligand complexes. In a nutshell, the input to this system is ligand from source S, and output is receptor ligand complex. Schematic representation of this model is shown in Figure D-1.

The various rates of change of species in the volume V are given according to equation D1,D2 and D3.

$$\frac{dR}{dt} = -k_{on}RL + k_{off}C - k_t R + Q_R \qquad \text{Eq. (D1)}$$

$$\frac{dC}{dt} = k_{on}RL - k_{off}C - k_e C \qquad \text{Eq. (D2)}$$

$$\frac{dL}{dt} = \frac{[-k_{on}RL + k_{off}C]}{N_{av}V} + f(t) \qquad \text{Eq. (D3)}$$

Appendix E

Axon Growth Model

It is known that neurotrophic gradients can be sensed by axon growth cones[30], which in turn allow the axon fibres to navigate their way through the tissue inorder to reach the target organs. The key parameters for axon growth in terms of chemical sensing are concentration gradient and concentration itself. The mathematical model mentioned below allows formulating an equation for axon growth rate[31]. This equation then can be coupled with the already developed physics in the computer model. The different parameters for this models are mentioned in Table E.1.

For simplicity, it is assumed that there is only one type of receptor that binds to receptor, with a dissociation constant of K_d. Furthermore, there would be an upper limit of concentration C_{max}, above which axon growth would not be affected (because of receptor saturation).

Assuming that the concentration in a channel is uniform, axons grow at a rate of Z_b um/s (equation E1).

$$\frac{\mathrm{dz}}{\mathrm{dt}} = \mathrm{Z_b} \qquad \text{Eq. (E1)}$$

Now, let us assume there is a concentration gradient present inside the conduit (such as in the differential coil configuration). The concentration gradient is only assumed in the axial direction. In such a scenario, axonal growth would occur because of two things[32]: 1) simply because of the drug present in the system; second, because of the drug concentration gradient. Therefore, equation E1 can be modified and written as:

$$\frac{dz}{dt} = Z_b + k\frac{dc}{dz} \qquad \text{Eq. (E2)}$$

Table E-1: Different parameters involved in axon growth model

z	Axial axon growth
c	NGF concentration in device
$\frac{\partial c}{\partial z}$	NGF concentration gradient at length 'x' um
k	Gradient steepness factor
Z_b	Baseline axonal growth rate with constant NGF concentration throughout
$C_{threshold}$	Threshold NGF concentration to trigger any axial growth
ΔC_t	Threshold concentration gradient below which growth equals as that caused by $C_{threshold}$
T_{lag}	Time lag between sensing chemotactic gradient and mechanical movement

If the time duration starting from a particular time 't' is less than T_{lag}, then $\frac{dz}{dt}$ is Z_b.

The term (dc/dx) can be estimated by the computer model based on localized axial gradient term, specifically "chds.gradz_c" as used in COMSOL Multiphysics. (The axial axis is the z-axis in COMSOL model).

References

1. Belkas JS, Shoichet MS, Midha R. Peripheral nerve regeneration through guidance tubes. Neurol Res. 2004 Mar;26(2):151-60. Review. PubMed PMID: 15072634.
2. Jason S. Belkas, Molly S. Shoichet, Rajiv Midha, Axonal guidance channels in peripheral nerve regeneration, Operative Techniques in Orthopaedics, Volume 14, Issue 3, July 2004, Pages 190-198, ISSN 1048-6666, http://dx.doi.org/10.1053/j.oto.2004.06.001.
3. Quigley AF, Bulluss KJ, Kyratzis IL, Gilmore K, Mysore T, Schirmer KS, Kennedy EL, O'Shea M, Truong YB, Edwards SL, Peeters G, Herwig P, Razal JM, Campbell TE, Lowes KN, Higgins MJ, Moulton SE, Murphy MA, Cook MJ, Clark GM, Wallace GG, Kapsa RM. Engineering a multimodal nerve conduit for repair of injured peripheral nerve. J Neural Eng. 2013 Feb;10(1):016008. doi: 10.1088/1741-2560/10/1/016008. Epub 2013 Jan 3. PubMed PMID: 23283383.
4. Johnson EO, Soucacos PN. Nerve repair: experimental and clinical evaluation of biodegradable artificial nerve guides. Injury. 2008 Sep;39 Suppl 3:S30-6. doi: 10.1016/j.injury.2008.05.018. Epub 2008 Aug 22. Review. PubMed PMID: 18722612.
5. Schmidt CE, Leach JB. Neural tissue engineering: strategies for repair and regeneration. Annu Rev Biomed Eng. 2003;5:293–347.
6. Bronzino, Joseph D.. The biomedical engineering handbook. 2nd ed. Boca Raton, FL: CRC Press, 2000. Print.
7. Mackinnon SE, Dellon AL. A study of nerve regeneration across synthetic (Maxon) and biologic (collagen) nerve conduits for nerve gaps up to 5 cm in the primate. J Reconstr Microsurg.1990;6(2):117–21

8. Li S, Archibald S, Krarup C, Madison R. Peripheral nerve repair with collagen conduits. Clin Mater 1992;9:195–200
9. Cao X, Shoichet MS. Defining the concentration gradient of nerve growth factor for guided neurite outgrowth. Neuroscience. 2001;103(3):831-40. PubMed PMID: 11274797.
10. Tansey KE, Seifert JL, Botterman B, Delgado MR, Romero MI. Peripheral nerve repair through multi-luminal biosynthetic implants. Ann Biomed Eng. 2011 Jun;39(6):1815-28. doi: 10.1007/s10439-011-0277-6. Epub 2011 Feb 24. PubMed PMID: 21347549.
11. Ramanujan S, Pluen A, McKee TD, Brown EB, Boucher Y, Jain RK. Diffusion and convection in collagen gels: implications for transport in the tumor interstitium. Biophys J. 2002 Sep;83(3):1650-60. PubMed PMID: 12202388; PubMed Central PMCID: PMC1302261.
12. Kyekyoon Kevin Kim, Daniel W. Pack. Microspheres for drug delivery. BioMEMS and Biomedical Nanotechnology 2006, pp 19-50
13. Kemp SW, Walsh SK, Midha R. Growth factor and stem cell enhanced conduits in peripheral nerve regeneration and repair. Neurol Res. 2008;30(10):1030–8.
14. Rosner BI, Siegel RA, Grosberg A, Tranquillo RT. Rational design of contact guiding, neurotrophic matrices for peripheral nerve regeneration. Ann Biomed Eng. 2003;31(11):1383–401.
15. Dontchev VD, Letourneau PC. Growth cones integrate signaling from multiple guidance cues. J Histochem Cytochem. 2003 Apr;51(4):435-44. Review. PubMed PMID:12642622.

16. Yeo Y, Park K. Control of encapsulation efficiency and initial burst in polymeric microsphere systems. Arch Pharm Res. 2004 Jan;27(1):1-12. Review. PubMed PMID: 14969330.
17. Murray JD. Reaction Diffusion, Chemotaxis and Non-local Mechanisms. Mathematical Biology: Springer; 1989. p. 232-53
18. Fournier RL. Basic transport phenomena in biomedical engineering. New York: Taylor & Francis, 2007
19. Leopold, Luna B., Wolman, M.G., and Miller, J.P., 1964, Fluvial Processes in Geomorphology, San Francisco, W.H. Freeman and Co., 522p
20. Mandelbrot B. How long is the coast of britain? Statistical self-similarity and fractional dimension. Science. 1967 May 5;156(3775):636–638
21. Katz MJ. How straight do axons grow? J Neurosci. 1985 Mar;5(3):589-95. PubMed PMID: 3973686.
22. Mandelbrot, Benoit B., and Carl J. G. Evertsz. Fractals and chaos: the Mandelbrot set and beyond. New York, NY [u.a.: Springer, 2004. Print.
23. Moore AM, Kasukurthi R, Magill CK, Farhadi HF, Borschel GH, Mackinnon SE. Limitations of conduits in peripheral nerve repairs. Hand (NY). 2009;4(2):180–6.
24. Korsching S, Thoenen H. Quantitative demonstration of the retrograde axonal transport of endogenous nerve growth factor. Neurosci Lett. 1983 Aug 19;39(1):1-4. PubMed PMID: 6195560.
25. Wiesmann C, de Vos AM. Nerve growth factor: structure and function. Cell Mol Life Sci. 2001 May;58(5-6):748-59. Review. PubMed PMID: 11437236.
26. Tani T, Miyamoto Y, Fujimori KE, Taguchi T, Yanagida T, Sako Y, Harada Y. Trafficking of a ligand-receptor complex on the growth cones as an essential step for the uptake of nerve growth factor at the distal end of the axon: a single-

molecule analysis. J Neurosci. 2005 Mar 2;25(9):2181-91. PubMed PMID: 15745944.

27. Chao MV. The p75 neurotrophin receptor. J Neurobiol. 1994 Nov;25(11):1373-85. Review. PubMed PMID: 7852992.
28. Shankaran H, Resat H, Wiley HS. Cell surface receptors for signal transduction and ligand transport: a design principles study. PLoS Comput Biol. 2007 Jun;3(6):e101. Epub 2007 Apr 20. Review. PubMed PMID: 17542642; PubMed Central PMCID: PMC1885276.
29. Cao X, Shoichet MS. Defining the concentration gradient of nerve growth factor for guided neurite outgrowth. Neuroscience. 2001;103(3):831-40. PubMed PMID:11274797.
30. Tse TH, Chan BP, Chan CM, Lam J. Mathematical modeling of guided neurite extension in an engineered conduit with multiple concentration gradients of nerve growth factor (NGF). Ann Biomed Eng. 2007 Sep;35(9):1561-72. Epub 2007 May 23. PubMed PMID: 17520368.
31. Kapur TA, Shoichet MS. Chemically-bound nerve growth factor for neural tissue engineering applications. J Biomater Sci Polym Ed. 2003;14(4):383-94. PubMed PMID: 12747676.
32. L. Ma and D.A. Gibson, Chapter 3 - Axon Growth and Branching, In Cellular Migration and Formation of Neuronal Connections, edited by John L.R. Rubenstein and Pasko Rakic, Academic Press, Oxford, 2013, Pages 51-68, ISBN 9780123972668.
33. Goldberg JL. How does an axon grow? Genes Dev. 2003 Apr 15;17(8):941-58. Review. PubMed PMID: 12704078.

34. Lauffenburger, Douglas A., and Jennifer J. Linderman. Receptors: models for binding, trafficking, and signaling. New York: Oxford University Press, 19961993. Print.
35. David D. Eveleth. Nerve growth factor receptors: Structure and function. In Vitro Cellular & Developmental Biology, 1988, Volume 24, Number 12, Page 1148.
36. Nesreen Zoghoul Alsmadi, Lokesh Patil, Elijah Hor, Parisa Lofti, Joselito M. Razal, Cheng-Jen Chuong, Gordon G Wallace, Mario I. Romero Ortega (2014). *Coiled Polymeric Growth Factor Gradients for Multiluminal Neural Chemotaxis.* Manuscript submitted for publication.
37. Martinez, E. (2011). Three-dimensional multimedium computational model for drug delivery using finite element analysis. (Order No. 1493891, The University of Texas at Arlington). ProQuest Dissertations and Theses, 69. Retrieved from http://ezproxy.uta.edu/docview/873456735?accountid=7117. (873456735).
38. Berger, Richard A., and Arnold Weiss. Hand surgery. Philadelphia: Lippincott Williams & Wilkins, 2004. Print
39. Frei, Walter. "COMSOL Blog." Meshing Your Geometry: When to Use the Various Element Types. COMSOL Inc, n.d. Web. 20 Apr. 2013.
40. Barrer, R. M. "Solutions of the diffusion equation ." Diffusion in and through solids,. Cambridge, Eng.: The University press;, 1941. 1-52. Print.

Biographical Information

Lokesh Shamkant Patil was born in Jalgaon, India on Dec 19th, 1988 and was raised in Gurgaon, India where he completed his schooling. Following his childhood interest in automobiles he enrolled in Bachelor of Science in Mechanical and Manufacturing Engineering at Manipal University, India. During his college, he went on to be part of two different race car designing teams; experiences which created his foundation in design engineering. Later, after graduating in May 2010, he lost a year to illness, during which he got interested in medicine and decided to pursue his Masters in Bioengineering at the University of Texas at Arlington with focus on Biomechanics. His goal in life is to use his skills as an engineer to contribute towards the field of affordable and quality healthcare. He has a strong interest in designing of medical devices that can be manufactured at low costs along with their commercialization to make them accessible to people in developing parts of world. He also plans to be part of organizations that help spread awareness about medical conditions, common as well as rare, to make early diagnosis and treatment options possible.